MAGNETIC RESONANCE IMAGING OF CEREBROVASCULAR REACTIVITY USING GAS INHALATION CHALLENGES

by

HARSHAN RAVI

Presented to the Faculty of the Graduate School of

The University of Texas at Arlington in Partial Fulfillment

of the Requirements

for the Degree of

DOCTOR OF PHILOSOPHY

THE UNIVERSITY OF TEXAS AT ARLINGTON

DECEMBER 2015

Acknowledgements

I have many people in my life to thank who helped shape my carrier. First and foremost I would like to thank my mentor Dr. Hanzhang Lu who accepted me as a part of his lab. I greatly appreciate his continuous guidance and support throughout my training. His guidance helped me all the time of research and writing of this thesis. I could not have imagined having a better advisor and mentor for my Ph.D study.

Besides my advisor, I would like to thank the rest of my thesis committee: Dr. Hanli Liu (chairperson), Dr.Marco Pinho, Dr. Xuejun Gu and Dr. Georgios Alexandrakis for their insightful comments and encouragement, but also for the hard question which incented me to widen my research from various perspectives. I would like thank my lab members/alumni Dr. Binu P Thomas, Dr. Shin-Lei Peng, Dr. Lisa Krishna Murthy, and friends Dr. Sandeep Ganji, Amarnath Yenuu and Gehna Mansinghani for providing expertise and help whenever needed and enlightening me with their insightful discussions.

Last but not the least, I would like to thank my family: my parents Chandra Sekhar Ravi, Jaya Lakshmi Ravi and my brother Vineel Ravi for supporting me emotionaspiritually throughout writing this thesis and my life in general.

November 12, 2015

Abstract

MAGNETIC RESONANCE IMAGING OF CEREBROVASCULAR REACITIVITY USING GAS INHALATION CHALLENGES

Harshan Ravi, PhD

The University of Texas at Arlington, 2015

Supervising Professor: Hanzhang Lu

Cerebrovascular reactivity (CVR) is a measure of dilation capacity of cerebral vasculature. It is an important biomarker for the vascular functionality and integrity, and may have clinical indications in stroke, atherosclerosis, Moyamoya disease, multiple sclerosis, brain tumor, and other neurological disorders. The most commonly used approach to measure CVR is by applying a physiological maneuver to alter the arterial carbon dioxide (CO_2) concentration (e.g. inhaling a small amount of CO_2 which is a potent vasodilator), while continuously acquiring BOLD MR images. However, the current method suffers from several limitations related to specificity, sensitivity, and physiological modeling of the measured signal. The goal of my thesis study is to improve on these aspects and ultimately provide a clinically-ready CVR imaging procedure that could

be immediately translational. The proposal's goals have been accomplished through the following specific aims:

Aim 1: Improve the specificity of CVR signal by optimization of imaging protocol.

Although positive CVR, i.e. increased BOLD signal with CO_2 inhalation, is expected in healthy brain, recently the presence of negative CVR has been reported using the current CVR imaging protocol, which can potentially compromise the interpretability of CVR data in clinical applications. In Aim 1, we performed simulation and experimental studies to provide a mechanistic understanding of this observation and showed that the negative CVR reported in the literature is an artifactual signal due to improper selection of imaging parameter. We further re-optimize the BOLD imaging parameters such that negative CVR is no longer present.

Aim 2: Improve the sensitivity of CVR mapping by applying a fast imaging technology, multiband MRI sequence.

CVR mapping inherently has low sensitivity as it relies on small BOLD signal changes in response to CO_2 inhalation, similar to fMRI. Recently, it has been shown that brain fMRI signal can be more robustly measured when using a fast imaging technology called multiband acquisition, and the technology has received wide attention. We hypothesize that multiband acquisition can also improve the sensitivity of

CVR data, by collecting images at a higher temporal resolution. In Aim 2, we examined the benefit of multiband acquisition in CVR mapping by comparing CVR data collected with multiband factor of 2 (imaging two times faster) and 3 (imaging three times faster) to those with regular acquisition.

Aim 3: Investigate modeling and nonlinearity issues in CVR data analysis.

The previous two aims examined data acquisition strategies in CVR mapping. The present aim focuses on issues related to data analysis. A linear relationship is usually assumed between EtCO2 and the BOLD signal, making linear model the most widely used model in CVR analysis. However, recent reports have suggested a nonlinear relationship between BOLD signal and arterial CO2 concentration. In Aim 3, we proposed an improved modeling scheme that incorporates possible nonlinearity while preserving the linear effect, through which we investigated the extent of nonlinear effect in CVR data and its dependence on age.

Table of Contents

List of Illustrations

List of Tables

Chapter 1

Introduction

1.1 Cerebral blood flow

Brain is highly metabolic and important organ of the body. Even though it weighs only 2% body weight, however, requires a disproportionate amount (~20 %) of the total blood flow. Unprecedented fall in cerebral blood flow (CBF) would quickly lead to unconsciousness and, if sustained for a longer period of time would result in brain damage and death. Therefore, CBF is tightly regulated in the brain, as it facilitates the delivery of essential substrates required for metabolism and removal of metabolic byproducts.

1.1.1 Mechanism regulating CBF

The cerebrovasculature is always under the combined influence of a number of physical and chemical stimuli that adjust vascular caliber/resistance so as to alter the blood supply to different parts of the brain (Bayliss, 1902; Lassen, 1959). Autoregulation and metabolic coupling are two important mechanisms which regulate the CBF in the brain. Autoregulation ensures that constant blood flow is supplied in the face of changes in perfusion pressure. The mechanism through which autoregulation controls the blood flow during pressure changes is thought to be myogenic in nature, but other factors such as metabolic (CO_2, O_2, and

so on) factors also assert some influence (Osol et al., 2002; Paulson et al., 1990; Peterson et al., 2011). Furthermore, metabolic coupling mechanisms ensure that blood flow increases in active regions. CBF is highly variable across the brain and largely dependent on neuronal activity, thus, an increase in neuronal activity causes an increase in the cerebral metabolic rate, which in turn results in proportional increases in blood flow (Paulson et al., 1990; Tameem and Krovvidi, 2013). The flow, metabolic coupling is influenced by metabolic, glial, neural, and vascular factors. The underlying mechanism regulating flow metabolism coupling taught to be mediated by various metabolites (adenosine, lactate, CO_2, H+, nitric oxide etc.) produced during the metabolic activity.

1.1.2 Influence of arterial blood gases on CBF

In general, arterial concentration of CO_2 and O_2 also have a profound influence on CBF regulation. Elevated levels of CO_2 in arterial blood results in the increase in CBF. The changes in CBF due arterial blood CO_2 are mediated through extravascular H+ ion changes. Both elevated and diminished levels of CO_2 are thought to have noxious effects on cerebral tissue. Therefore, Arterial hypercapnia, by increasing cerebral perfusion, facilitates the disposal of CO_2 produced by the brain and, arterial hypocapnia, by decreasing cerebral perfusion restricts the CO_2 loss from the brain. Furthermore, the arterial partial pressure of CO_2 also plays has a

strong influence on autoregulation plateau; shortening of the autoregulation plateau with hypercapnia and lengthening of autoregulation plateau during hypocapnia state (Meng and Gelb, 2015). On the other hand, inhalation of air mixtures of low oxygen concentration causes dilation of the pial arteries, whereas high arterial oxygen concentration cause a moderate vasoconstriction. During, hypoxia oxygen-sensitive ion channels in the vascular smooth muscles are activated and vasoactive substances, such as Nitric oxide, adenosine are released (Paulson et al., 1990). These metabolic factors are responsible for the vasodilatation and increases in CBF. Opposite effect is observed during elevated levels of oxygen. Overall, arterial concentrations of blood gases CO_2 and O_2 serves to control the distribution of cerebral blood flow. EtCO2 is used as a physiological marker for arterial CO_2 concentration changes.

1.1.3 EtCO2 as a surrogate for arterial concentration of CO_2

EtCO2 is a quantitative measure, which represent the partial pressure or concentration of CO_2 at the end of an exhaled breath and it is expressed in units of percentage of CO_2 or mmHg. Cells in the human body requires energy to sustain day to day activity and the energy required for activity is generated through metabolism. CO_2 is one of the major byproducts of metabolism. Elevated levels of CO_2 are continuously removed from the body through a process called respiration. As the

intracellular CO_2 levels increase, CO_2 diffuses into the capillaries and is carried by the venous circulation to the lungs, where it diffuses from pulmonary capillaries into the alveoli. Ventilation of the lungs is the process that mixes fresh, inspired gas with alveolar gas. In general, the partial pressure of CO_2 (PvCO2) of venous blood entering pulmonary capillaries is higher than the partial pressure of CO_2 (PACO2) of alveoli. This pressure gradient will cause CO_2 to diffuse out of pulmonary capillaries into the alveoli. CO_2 is then eliminated by alveolar ventilation under the control of the respiratory center *(Donald and Paterson, 2006).* EtCO2 reflects ventilation (lung function), circulation (cardiac function), and metabolism. Under normal physiologic conditions the EtCO2 value closely follows the changes in arterial CO_2 concentration. Therefore, EtCO2 used as a surrogate for arterial blood CO_2 changes. Most commonly used method used by investigators to probe into the regulation of cerebral blood flow and its distribution is to subject the system with a vasoactive stimuli such as CO_2 and observed its response. Such an experiment leads to the measurement of cerebrovascular reactivity (CVR).

1.2 Cerebrovascular reactivity (CVR)

The brain vascular system is divided into two branches. A supplying (arterial) branch and draining (venous) branch as shown in Figure 1-1 (Harrison et al., 2002). The arterial vasculature is surrounded by smooth

muscles (represented by an asterisk in Figure 1-1). When a vasodilatory stimulus is presented to the arterial vasculature they dilate, increasing the CBF to that region. Cerebrovascular reactivity (CVR) reflects the ability of the brain vasculature to dilate in response to a vasodilatory stimulus. CVR is an important biomarker for vascular reserve capacity (Yezhuvath et al., 2009b). CVR can give a wealth of information beyond baseline cerebral blood flow (CBF) and cerebral blood volume (CBV) measures (Kassner et al., 2010) and have demonstrated important utility in cerebrovascular pathologies (Fierstra et al., 2011; Karapanayiotides et al., 2004; Mandell et al., 2008a; Mikulis et al., 2005; Vernieri et al., 2001; Ziyeh et al., 2005).

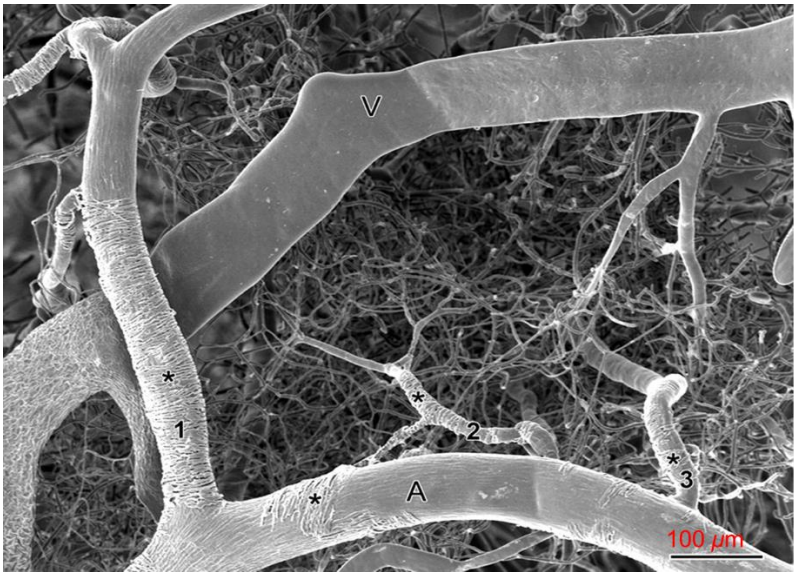

Figure 1-1 Illustration of cerebral vasculature. The arterial vasculature is represented with A and venous vasculature with V. smooth muscle lining is indicated by asterisk.

During a CVR measurement the subject is presented with a hypercapnia (5 % CO2) stimulus, and this would elicit vasodilation and ultimately result in CBF increase. A perfusion sensitive imaging technique is used to measure the CBF changes. A linear regression between measured EtCO2 and vascular response would give CVR.

1.3 Imaging CVR

1.3.1 Carbon dioxide modulation of cerebral blood flow during gas inhalation challenge

Many vasodilatory stimulus are suggested in the literature for CVR measurement such as breath hold, acetazolamide, varying minute ventilation and hypercapnia. However, the most widely used vasoactive stimulus is 5% CO_2 or hypercapnia gas. Hypercapnia has profound and reversible effect on CBF. Hypercapnia causes dilation of cerebral vasculature and increases blood flow, on the other hand hypocapnia causes vasoconstriction and decreases blood flow. The CO_2 concentration changes in arterial blood are measured using EtCO2. Although several mechanisms have been proposed for hypercapnic vasodilation, however, till date, the major mechanism for CBF modulation is thought to be a direct effect of extracellular H+ ions on vascular smooth muscle. The increased EtCO2 leads to increased concentration of extravascular H+ ions, which triggers voltage gated K+ channels resulting in hyperpolarization of smooth

muscle cells. This would result in a reduction of intracellular calcium, causing vascular relaxation and hence vasodilatation (Paulson et al., 1990). EtCO2 is used as a surrogate for arterial CO_2 concentration. It is commonly assumed that, during hypercapnia, the relationship between EtCO2 and blood flow change is linear. That is, one can write cerebrovascular reactivity in units of percent CBF change per mmHg change in EtCO2. However, some reports have suggested that CBF may increase at an accelerated rate at high EtCO2 levels (Kastrup et al., 1997; Markwalder et al., 1984).

1.3.2 Magnetic Resonance Imaging of CVR using gas inhalation challenges

Many neuro imaging techniques have been used for CVR mapping. A few of the notable techniques used in CVR measurement are Trans Cranial Doppler ultrasonography (TCD) (Kuroda et al., 2001), Positron Emission Tomography (PET) (Ogasawara et al., 2003), single Photon Emission Computed Tomography (SPECT) (Kuroda et al., 2001) and Near Infrared Spectroscopy (NIRS) (Smielewski et al., 1995). Although TCD & NIRS provide excellent temporal resolution but provide low spatial resolution and whole brain coverage. On the other hand, PET and SPECT even though offers full brain coverage but suffer from high cost, limited spatial resolution, technical difficulty, use of intravenous radioactive tracers, and exposure to radiation (Leoni et al., 2012). The most commonly used

technique to evaluate cerebral hemodynamics with whole-brain coverage is magnetic resonance imaging (MRI).

Magnetic Resonance Imaging (MRI) developed at the end of the 20th century has shown tremendous growth and the potential for improvement in terms of speed, robustness, and reproducibility. The most important advantages of using MRI are good spatial resolution, whole brain coverage and the feasibility to be customize for clinical and research objective under investigation. As such MRI can be conveniently tailored to measure CBF changes during CVR measurements. Recently, use of MRI to study and understand cerebrovascular physiology gained prominence in the research community.

1.3.3 Origin of blood oxygen level dependent (BOLD) MRI signal changes during gas inhalation challenge

Blood oxygen level dependent (BOLD) MRI is most commonly used technique to measure CVR (Thomas et al., 2013). BOLD MRI is a non-invasive imaging method which uses indigenous deoxy-hemoglobin concentration to measure CBF changes in the microvasculature (Ogawa et al., 1990). During CVR measurement, the hypercapnia stimulus given to a subject would elicit vasodilation in cerebrovasculature and this would result in a subsequent CBF increase. The increase in CBF would bring more oxygen to the brain than required for metabolism and this would result in

deoxyhemoglobin concentration decrease. Deoxy-hemoglobin is paramagnetic in nature and distorts the local magnetic field (filed distortion is depicted as dark shadow around the venule in Figure 1-2a). Therefore, a reduction in deoxy-hemoglobin concentration results in less local field distortion as shown in Figure 1-2b, and this would result in increased BOLD signal. Conversely, a reduction in CBF would result in increased deoxy-hemoglobin concentration which distorts the local magnetic field and consequently result in decreased BOLD signal.

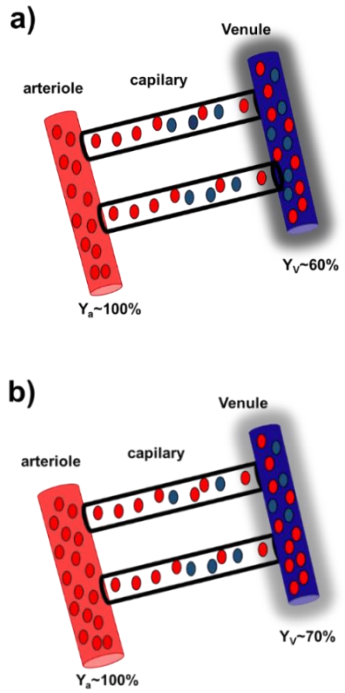

Figure 1-2 Graphical illustrations of fractional changes in oxyhemoglobin concentration relative to deoxy hemoglobin concertation. a) baseline and b) hypercapnia stimulus.

The information acquired from CVR mapping in the healthy population, therefore can be used to differentiate between healthy and pathological condition. Figure 1-3 shows a CVR map of a moyamoya patient suffering from unilateral impairment. Note that there is a clear distinction between CVR preserved (yellow) region and CVR impaired (blue) region. The blue region corresponds to negative CVR. The observed negative CVR is associated with vascular steal phenomenon, where the CBF from CVR impaired (blue) region is stolen and distributed to CVR preserved (yellow) region under the influence of vasoactive stimulus. So, in the healthy vasculature (yellow) the CBF increases, resulting in increased oxy hemoglobin concentration and overall increase in MR signal, simultaneously in the diseased vasculature (blue) the CBF decreases, resulting decrease in oxyhemoglobin concentration and decreased signal.

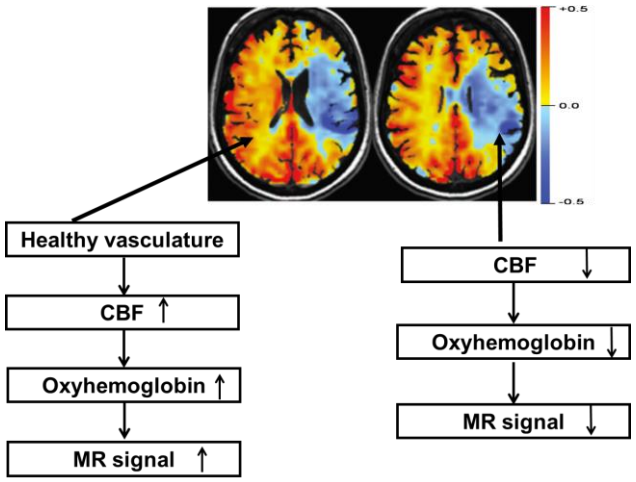

Figure 1-3 CVR map of a stenooclusive patient suffering from unilateral impairment. The blue region represent CVR impaired region and yellow region CVR preserved region. Adopted from (Mandell et al., 2008a).

1.3.4 Experimental set up

A typical experimental setup used for CVR measurement is shown in Figure 1-4. The subject is fitted with a mouthpiece and a nose clip. This would facilitate the breathing through the mouth. The end of the mouth piece is connected to a long hollow tube and the other end of this tube is connected to a two way valve. One end of this valve connected to the Douglas bag and the other end is left open to facilitate the room air breathing. The Douglas contains the gas mixture used in the experiment.

Figure 1-4 Illustration of experimental setup used in typical CVR measurement

1.4 Significance

1.4.1 Optimization of imaging protocol for the mapping of cerebrovascular reactivity (CVR)

Brain weighs only 2% of the total body weight, but requires about 20% of the total body energy requirement. It doesn't have the capacity to store the substrates and requires constant supply of the substrates for metabolism. Blood provides necessary substrates required for metabolism, therefore the adequate functionality of cerebral vasculature is required for proper functioning of the brain. Investigators use CVR to evaluate the vitality of brain vasculature. The most commonly used approach to measure CVR

is by applying a physiological maneuver to alter the arterial carbon dioxide (CO2) concentration (e.g. inhaling a small amount of CO2, which is a potent vasodilator), while continuously acquiring BOLD MR images (Gauthier et al., 2012; Kastrup et al., 2001; Rostrup et al., 2000; Thomas et al., 2013; Yezhuvath et al., 2009b). A logical expectation is that increase in arterial CO_2 concentration results in an increase in BOLD signal (i.e. positive CVR) for healthy vasculature. A blunted response or, moreover, a decreased BOLD signal (i.e. negative CVR) would then indicate diseased vasculature. However, a few recent studies have reported negative CVR in the healthy brain vasculature (Blockley et al., 2011; Mandell et al., 2008a; Thomas et al., 2013), clouding the interpretation of this promising technique. Mandel et al. observed that negative CVR is present in the deep white matter (Mandell et al., 2008a) . Blockley et al. showed that negative CVR was mainly observed in the cerebrospinal fluid (CSF) rich ventricular region (Blockley et al., 2011). Thomas et al. (Thomas et al., 2013) explained the mechanistic reasoning for the appearance of negative CVR in healthy brain vasculature. It was shown that the presence of negative CVR in healthy brain is due to displacement of CSF by the dilation of blood vessels. Since CSF signal is bright in a typical BOLD image, this reduction of CSF partial volume during vasodilation results in an artifactual decrease in BOLD signal in a voxel, independent of any oxygenation changes. In AIM 1, we reoptimized the

BOLD imaging protocol to attenuate the artifactual negative CVR. Negative CVR has been previously reported in patients with cerebrovascular diseases as evidence of a loss of vascular reserve (Fierstra et al., 2011; Mikulis et al., 2005). However, the presence of artifactual signal source could cloud the interpretation of such results. Similarly, negative CVR has been proposed as a guide for presurgical planning in brain tumors (Zaca et al., 2011b). However, in light of the “volume effect”, caution should be taken when interpreting such findings as the tumor may be adjacent to CSF-filled edema regions, which contain large amount of fluid. Therefore, the optimized BOLD protocol could remove the “volume effect” and ascertain the correct identification of tumor territory.

1.4.2 Multiband BOLD acquisition enhances the sensitivity of cerebrovascular reactivity (CVR) mapping

Cerebrovascular reactivity (CVR) reflects the ability of the brain vasculature to dilate in response to a vasoactive stimulus (Yezhuvath et al., 2009b). CVR can give a wealth of information beyond baseline CBF and cerebral blood volume (CBV) measures, and have demonstrated an important utility in evaluating the brain vascular disorders (Fierstra et al., 2011; Greenberg, 2006b; Mandell et al., 2008a; Mikulis et al., 2005). BOLD MRI based technique is most commonly used procedure to measure CVR (Thomas et al., 2013). However, like other functional and physiological

indices (Ramsey et al., 1996), the biggest drawback of BOLD MRI is its poor sensitivity and reliability. The low sensitivity in BOLD measurements stems from inherently small signal changes observed during hypercapnia experiment, which are only a few fractions (1~3%) of the total signal. The detection sensitivity of these small signal changes are further confounded by the presence of noise sources (de Zwart et al., 2008). One way to improve the sensitivity is averaging multiple CVR scans or scanning for a long time, both of the strategies would lead to increased scan time, thereby increasing patient discomfort. Similar sensitivity improvement can be achieved by decreasing repetition time (TR) i.e. faster acquisition rate. However, deceased TR would result in decreased brain coverage. Multiband EPI has shown strides of improvement in acquiring whole brain coverage with reduce TR. Multiband EPI is a fast-imaging technology that allows the excitation and acquisition of multiple 2D slices simultaneously (Feinberg et al., 2010; Setsompop et al., 2012). In fMRI and DTI applications, it has been shown that multiband EPI provides an SNR advantage over single-band (conventional) EPI, owing to its higher temporal sampling rate(Feinberg et al., 2010). In Aim2, we investigated the sensitivity improvement for CVR mapping using multiband acquisition and to our knowledge this is first of its kind attempt to improve the sensitivity of CVR mapping. CVR is an important biomarker for cerebrovascular reserve and

has been increasingly used in the studies to evaluate the cerebrovascular diseases. Most recently, it has been used in previously unexplored territories such as presurgical planning and evaluation of patient outcome post-surgery. Improved sensitivity using multiband acquisition could be used to acquire high resolution data or reduce the scan time.

1.4.3 An investigation on nonlinearity in BOLD response during the moderate hypercapnia challenge

As discussed above, the changes in arterial CO_2 concentration modulates the CBF changes. In CVR experiments a linear relationship is assumed between hypercapnia induced EtCO2 change and the resultant change in the CBF/BOLD signal. However, investigations of CVR using TCD in combination with progressively increasing ramp hypercapnia stimulus have shown a nonlinear relationship between cerebral blood flow velocity and arterial CO_2 partial pressure (PaCO2) (Battisti-Charbonney et al., 2011; Claassen et al., 2007). A non-linear CVR relationship will complicate the interpretation of BOLD based CVR results. However, in all the studies discussed above the stimulus used was a ramp stimulus, starting from hypocapnic state to hypercapnic state. In general, the stimulus range used in those experiments is above the normal range of stimulus used in clinical settings and could potentially cause discomfort to the patients. In Aim 3, we investigated the nonlinearity in the BOLD response

to moderate hypercapnia challenge. We proposed an improved modeling scheme that incorporates possible nonlinearity while preserving the linear effect, through which we investigated the extent of nonlinear effect in CVR data and its dependence on age. The slope of the linear component now accurately represents the CVR

Chapter 2

Optimization of imaging protocol for the mapping of cerebrovascular reactivity

2.1 Introduction

Cerebrovascular reactivity (CVR) measures the dilatory capacity of cerebral vasculature to a vasoactive stimulus (Bhogal et al., 2014; Hare et al., 2013; Lipp et al., 2015; Mark et al., 2015; Mikulis et al., 2005; Tancredi and Hoge, 2013; Tancredi et al., 2015; Yezhuvath et al., 2009). It is an important marker for vascular reserve and has crucial implications for cerebral vascular integrity and functionality (Kety and Schmidt, 1948). Compared to baseline perfusion and cerebral blood volume (CBV), CVR is thought to be a more specific marker for cerebrovascular diseases (Kassner et al., 2010). Thus, availability of such a biomarker could be a useful tool in assessing and understanding many cerebral and cerebrovascular pathologies such as arteriovenous malformation (Fierstra et al., 2011a), small vessel diseases (Greenberg, 2006), cerebral proliferative angiopathy (Fierstra et al., 2011b), moyamoya disease (Donahue et al., 2013; Mikulis et al., 2005), arterial stenosis(Marshall et al., 2014), drug addictive condition (Han et al., 2008), multiple sclerosis(Marshall et al., 2014), cerebral gliomas(Hsu et al., 2004) and Alzheimer's disease (Glodzik et al., 2013; Yezhuvath et al., 2012). Additionally, it has been used to study the impact

of pharmacological agents on cerebral vasculature (Pattinson et al., 2007) and has also been suggested to be important in presurgical planning of brain tumor patients (Zaca et al., 2011). However, before this tool can be fully translated to clinical applications, optimization of imaging acquisition schemes is necessary.

The most commonly used approach to measure CVR is by applying a physiological maneuver to alter the arterial carbon dioxide (CO_2) concentration (e.g. inhaling a small amount of CO_2 which is a potent vasodilator), while continuously acquiring Blood-Oxygenation-Level-Dependent (BOLD) MR images (Gauthier et al., 2012; Halani et al., 2015; Kastrup et al., 2001; Lu et al., 2014; Rostrup et al., 2000; Yezhuvath et al., 2009). A logical expectation is that increase in arterial CO2 concentration results in an increase in BOLD signal (i.e. positive CVR) for healthy vasculature. A blunted response or, moreover, a decreased BOLD signal (i.e. negative CVR) would then indicate diseased vasculature. However, the interpretation of negative CVR data is not entirely straightforward (Blockley et al., 2011; Mandell et al., 2008; Thomas et al., 2013). Mikulis et al. reported the observations of negative CVR in Moyamoya patients (Mikulis et al., 2005). However, even though the stenosis affects the right hemisphere only, negative CVR regions were also detected in the left hemisphere, particularly in the deep brain regions (Mikulis et al., 2005).

Mandell et al. observed that negative CVR is present in the deep white matter of young, healthy individuals, close to posterior horns of the ventricle (Mandell et al., 2008). The question is then whether this represents a true "stealing effect" occurred even in healthy subjects, or it represents an imaging artifact. Blockley et al. showed that negative CVR was mainly observed in the cerebrospinal fluid (CSF) rich ventricular region (Blockley et al., 2011). The mechanistic reason for these observations was examined recently by Thomas et al. (Thomas et al., 2013). It was shown that the presence of negative CVR in healthy brain is due to displacement of CSF by the dilation of blood vessels in the voxel. Because CSF signal is bright in a typical BOLD image, this reduction of CSF partial volume during vasodilation results in a decrease in BOLD signal, independent of any oxygenation changes. Since, this negative signal change is due to physiological mechanisms other than perfusion or oxygenation increases, it is considered an artifact as far as CVR interpretation is concerned.

2.2 Methods

2.2.1 Theoretical study

Theoretical simulations in the present study were conducted in two steps, for two hypothetical voxels, respectively. In the first step, our goal was to identify all possible combinations of TR, TE and flip angle (FA) that could yield an artifact-free CVR result. This step was performed based on a

hypothetical voxel containing CSF and blood, as previous work has shown that such negative CVR artifacts are most pronounced in ventricular voxels. The second step asks the question, among the possible parameters identified above, which ones have the least penalty, if any, on sensitivity in a typical parenchyma voxel. Thus, the second simulation was performed on a hypothetical voxel containing parenchyma.

To address our first aim, we used a two-compartment model to study the BOLD signal in the ventricular regions. In this model, the imaging voxel was assumed to contain a combination of CSF and blood, with volume fraction of f_{CSF} and $(1-f_{CSF})$, respectively. The total BOLD signal in the voxel is given by:

$$S = f_{CSF} * S_{CSF} + (1 - f_{CSF}) * S_{blood} \quad [1]$$

where S_{CSF} and S_{blood} are MR signal per unit volume from CSF and blood compartment respectively. The unit-volume MR signal is in turn given by:

$$S_i = C_i * \frac{(1 - e^{\frac{TR}{T_{1,i}}})}{1 - \cos(FA) * e^{\frac{TR}{T_{1,i}}}} * \sin(FA) * e^{\frac{TE}{T^*_{2,i}}} \quad [2]$$

In the equation above, i could be CSF or blood. C is water density. TR, TE and FA represent repetition time, echo time and flip angle, respectively.

In an ideal BOLD-CVR experiment, the MR signal in Eq. [1] is assumed to be exclusively sensitive to T_2^*. However, when S_{CSF} and S_{blood} are not equal as in the case when conventional fMRI acquisition parameters are used, the total signal, S, is also affected by changes in f_{CSF}. This was the reason for the negative CVR observed in previous reports. To make the signal insensitive to the "volume effect", the following relationship needs to be satisfied:

$$S_{CSF} = S_{blood} \quad [3]$$

One can therefore solve Eqs. [2] and [3] to identify imaging parameter sets that can yield CVR maps absent of negative artifacts. In Eqs. [2] and [3], the MR property parameters are considered known variables and their assumed values are listed in Table 2-1. The unknown variables are TR, TE, and FA. Since there are multiple unknown variables in the equations, the solution is not unique. Therefore, the outcome after completing the first aim of our simulations is a two-dimensional parameter (TR and TE) set within which the blood and CSF signals are equated. The associated FA is also obtained.

Table 2-1 Parameters assumed in the simulation. C is the water density.

	C (ml/ml)	T1 (ms)	$T2^*$ (ms)
CSF	1[a]	3700[c]	1082.5[f]
Blood	0.87[a]	1624[d]	44.8[g]
Gray matter	0.83[b]	1445[e]	47[h]

[a] (Lu et al., 2002),

[b] (Whittall et al., 1997),

[c] (Clare and Jezzard, 2001),

[d] (Lu et al., 2004a),

[e] (Chen et al., 2001),

[f] (Lu et al., 2004b),

[g] (Zhao et al., 2007),

[h] (Lu and van Zijl, 2005)

The second aim of the theoretical studies is to determine the imaging parameters that produce highest sensitivity and also meet the criteria of absence of negative artifact. We therefore calculated an index, contrast to noise ratio per unit time (CNR), for a hypothetical gray matter voxel, the signal of which takes the form of Eq. [2]. Using gray matter parameters

assumed in Table 2-1, one can simulate the MR signal, S_{gray}, for any TR, TE, and FA. The CNR per unit time is given by:

$$CNR = \frac{SNR * CVR}{\sqrt{TR}} = \frac{S_{gray} * TE}{\sqrt{TR}} \quad [4]$$

In Eq. [4], SNR is replaced by S_{gray} assuming that the noise is independent of TR or TE. CVR is replaced by TE because they are linearly related to each other, for a given ΔR_2^*. The division by square-root of TR allows the conversion to unit time value, i.e. number of images for a given scan duration is accounted for. CNR is computed for each imaging parameter set and the set that corresponds to maximum CNR value is determined.

The outcome after completing the second aim of our simulations is that, at each TR, an optimal TE that yields the highest CNR is calculated. Across different TRs, the value that gives the highest CNR could also be calculated. But note that TR is also constrained by other factors such as spatial coverage and number of slices.

2.2.2 Experimental study

Experimental study was performed based on the results of the theoretical investigations. Specifically, within the two-dimensional parameter space of TE and TR, we chose three representative combinations. One protocol is the standard BOLD protocol, labeled as

“standard”, which is a typical protocol used in fMRI and previous CVR studies (Thomas et al., 2013) (black square in Figure 2-2c, TR/TE=1500ms/30ms). A second protocol, “Opt1”, is used to optimize TE and is a protocol using the same TR as the standard one but its TE is chosen to meet two criteria: 1) signals of blood and CSF are equated (thus no artifact of negative CVR); 2) CNR is the highest among all possible TEs at that TR. This protocol corresponds to the red triangle in Figure 2-2c. A third protocol, “Opt2”, is used to examine the TR dependence and is a protocol using a shorter TR of 800 ms with the TE chosen to again meet the two criteria described above. This corresponds to the red circle in Figure 2-2c.

The order of the three protocols was randomized for each subject. Two sessions were performed for each subject to test the reproducibility of the three protocols. The two sessions were carried out on the same day, but the participant was allowed to come out of the scanner and take a break before entering it again. The total gas-challenge scan duration for each participant was approximately 60 minutes, divided into two sessions of approximately 30 minutes each.

All experiments were performed at 3T (Philips Healthcare, Best, The Netherlands) using a body coil for transmission and a 32 channel head coil for receiving. The protocol has been approved by the Institutional Review

Board (IRB) of UT Southwestern Medical Center and all volunteers gave written informed consent before participating. The volunteers were all fitted with foam pads to reduce head motion. Ten healthy volunteers (age 29±8 years, 6 Female & 4 Male) were recruited to participate in this study.

The CVR measurement was performed using a CO_2-inhalation paradigm described previously (Yezhuvath et al., 2009a). The subject was fitted with a nose clip and a mouthpiece to allow mouth breathing. The subject inspired room air and the hypercapnic gas in an interleaved fashion (50 sec CO_2 followed by 70 sec room air, repeated four times with additional 45 sec room air inhalation at the end). The composition of the hypercapnic gas was 5% CO_2, 74% N_2 and 21% O_2. A research assistant was always present inside the scanner room during the experiment to monitor the subject and switch the valve that controls delivery of hypercapnic gas and room air. End-tidal CO_2 (EtCO2), which measures the concentration of CO_2 in the lungs and represents a surrogate for concentration of CO_2 in the arterial blood, was recorded for the entire duration of the scan using a capnograph device (Capnogard, Model 1265, Novametrix Medical Systems, CT). The duration of each CVR scan was 9 minutes.

Other BOLD imaging parameters were: field-of-view (FOV)=220x220 mm^2, matrix=64x64, thickness=5 mm, no gap between slices, the slice number was 28 for the “standard” and “Opt1” protocols, but was 18 for the

"Opt2" protocol due to a shorter TR used. Although Opt2 only provides partial brain coverage with 18 slices, we included this protocol in our testing because future studies using fast imaging techniques such as multiband EPI could provide more coverage at this TR.

2.2.3 Data analysis

BOLD data were processed using the Statistical Parametric Mapping (SPM) software, (University College London, UK) and in-house MATLAB (MathWorks, Natick, MA) scripts. Pre-processing included realignment of BOLD images, normalization to Montreal-Neurological-Institute (MNI) template EPI images with a resolution of 2x2x2 mm^3, and finally smoothing using a 6mm full width half maximum (FWHM) Gaussian kernel.

BOLD signal lags behind the EtCO2 time course, which is the input function to the cerebral vasculature. The $EtCO_2$ time-course was therefore shifted by a delay so that it is matched with the timing of the BOLD time-course. This delay represents the transit time for the blood to travel from the lung to the heart then to the brain, and it was computed on a subject-by-subject basis based on an algorithm described previously (Yezhuvath et al., 2009a).

For each subject, a General Linear Model (GLM) was used to calculate voxel-by-voxel CVR in units of % BOLD signal change per mmHg CO_2. In this model, the Et-CO_2 time-course was the independent variable

and the BOLD time-course was the dependent variable. Group-level one sample t test was then performed to identify voxels with significantly negative CVR using a family-wise-error (FWE) corrected $p<0.01$.

CNR per unit time, which represents the overall sensitivity of the CVR measurement, and coefficient of variation (COV), which represents the reproducibility, were also calculated by:

$$CNR = \frac{SNR * CVR}{\sqrt{TR}} \quad [5]$$

$$SNR = \frac{\mu_{baseline}}{\sigma_{baseline}} \quad [6]$$

$$COV = \frac{\sigma_{\text{inter}}}{\mu_{\text{inter}}} \quad [7]$$

where $\mu_{baseline}$, and $\sigma_{baseline}$ are average and standard deviation of baseline BOLD signal respectively. In addition, μ_{inter} and σ_{inter} represent intersession average and standard deviation, respectively.

2.2.4 Statistical analysis

To compare data across scan protocols, we performed one-way analysis of variance (ANOVA) tests with repeated measures of scan protocols on mean of CVR, SNR, CNR, and COV. If a scan protocol effect was observed in the ANOVA analysis, we used post-hoc scheffe's tests to

further compare the scan protocols in pairs. A multiple-comparison-corrected p value of 0.05 or less was considered significant.

2.3 Results

2.3.1 Theoretical study

Figure 2-1 a shows the imaging parameter sets (TR, TE, and the associated FA) that meets the criteria of absence of negative artifact. That is, if the BOLD imaging protocol is chosen to be any TR/TE/FA set on the plot, there should be minimal appearance of negative CVR voxels in the map. It can be seen that not all TR and TE combinations would yield a valid parameter set (e.g. white region in Figure 2-1a). That is, when TR and TE take on these values, the CSF and blood signal intensities cannot be matched no matter how one chooses the FA. Figure 2-1b shows the corresponding CNR per unit time. It can be seen that CNR varies considerably depending on TR and TE. It tends to be that, for a given TR, larger TE yields a greater CNR, but not always the case. Since TR is usually constrained by other considerations (e.g. number of slices, brain coverage) whereas TE is more flexible, we determined, for each TR, the optimal TE that yields the highest CNR. The results are shown in Figure 2-1c. It is evident from plot that the shorter the TR, the longer the optimal TE. However, all optimal TE are shorter than the typical TE values of 30-50 ms used in typical fMRI experiments. That is, in order to minimize the negative artifacts, the TE in a

CVR experiment needs to be shortened. We also examined the dependence of CNR on TR (at the respective optimal TE) (Figure 2-1d). It can be seen that shorter TR generally yields a greater CNR. Note, however, that TR is often constrained by the number of slices needed to cover the whole brain.

Experiments were therefore performed using two optimal imaging parameter sets suggested by Figure 2-1c (red symbols). One parameter set, referred to as “Opt1”, used TR/TE=1500 ms/21 ms, FA=89°. A second set, referred to as “Opt2”, used TR/TE=800 ms/22.5 ms, FA=72°. For comparison, we also collected data using a standard BOLD protocol, TR/TE=1500 ms/30 ms, FA=60° (black symbol in Figure 2-1c).

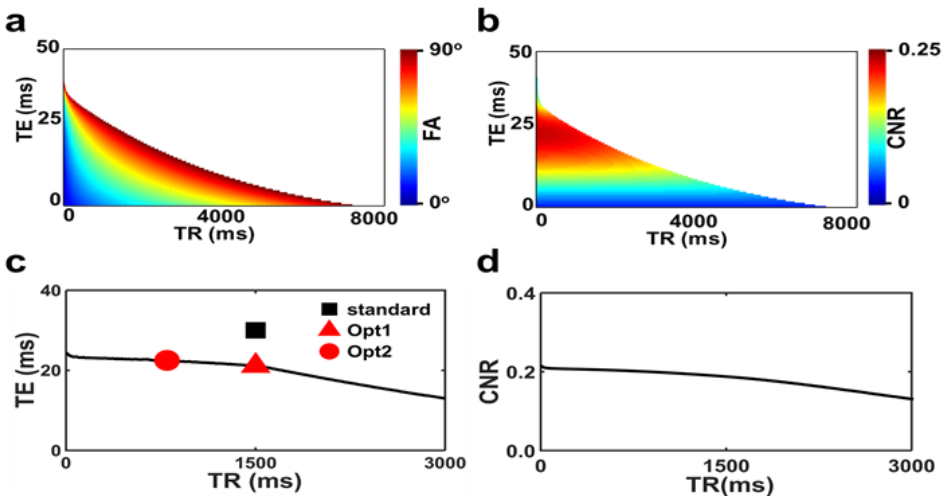

Figure 2-1 Simulation results from the theoretical study. (a) All possible combinations of TR, TE, and FA values that can equate the CSF and blood signal intensities in the BOLD image. The TR and TE values are represented on the x and y axis, respectively, and the FA value is represented by color scale. Note that, the imaging parameter space is divided into 2 distinct regions. The white region indicates that such TR and TE combination will not meet the signal equivalence criterion regardless the FA value. These results are obtained from step 1 of the simulation. (b) Corresponding CNR per unit time in a hypothetical parenchyma voxel. These results are obtained from step 2 of the simulation. (c) Optimal TE value as a function of TR. The symbols represent TR/TE combinations tested in the experiment. A total of three protocols were used: two using the optimized protocols with different TRs (red symbols) and one using the standard protocol (black symbol). With this strategy, both the TE and TR dependence of the CNR are examined. (d) CNR as a function of TR. For each TR, the optimal TE (and associated FA) was used to compute the CNR.

2.3.2 Experimental study

Figure 2-2a illustrates group-averaged BOLD images for the three protocols tested. It can be seen that, in the standard protocol, the MR signal in the ventricular region is brighter than the rest of the brain, confirming the notion that is greater than when typical BOLD protocol is used. In the optimized protocol, on the other hand, the difference between CSF and parenchyma is much less apparent, in accordance with the optimization criteria. Group-averaged CVR maps are shown in Figure 2-2b. The color scale is selected such that negative CVR is represented in cool colors and positive CVR is represented in warm colors. As expected, CVR map using the standard protocol shows considerable negative CVR voxels in the ventricular region (arrows in Figure 2-2b). In contrast, negative CVR is minimized when using the two optimized protocols (Figure 2-2b). Comparing CVR maps between session 1 and session 2 (Figure 2-2b), it appears that the results show excellent reproducibility.

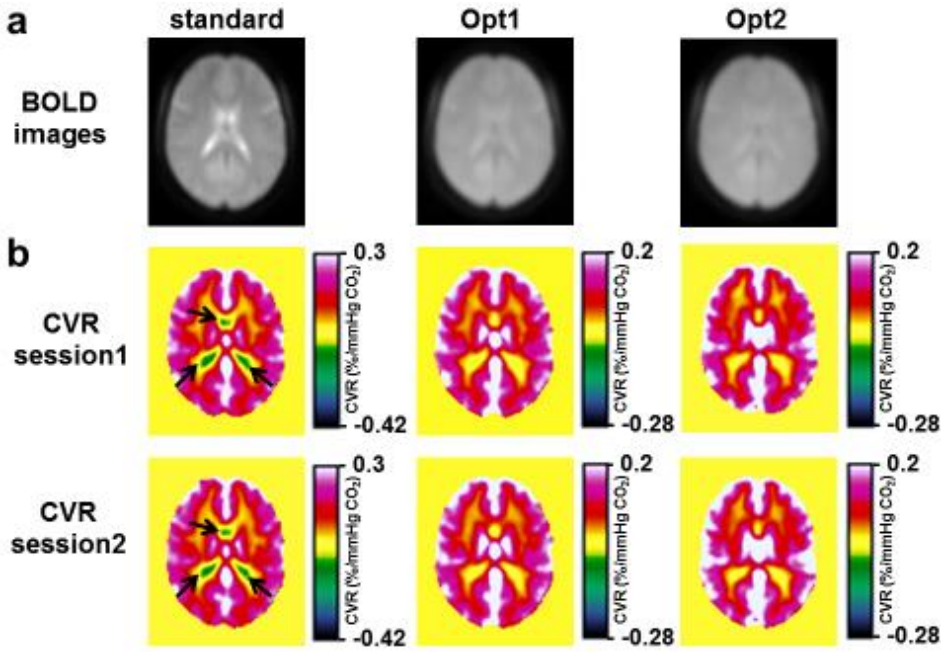

Figure 2-2 Group-averaged CVR results (N=10). (a) BOLD images in a representative slice (z=46 in MNI template) from the three protocols. Note that CSF-rich ventricles are bright in the standard protocol but not so in the optimized protocols (b) CVR maps from the three protocols for both sessions. The color bar is selected such that negative CVR voxels are generally represented in cool colors and positive CVR is represented in warm colors. The center of the color bar is slightly shifted toward the negative range to allow small negative CVR values due to noise, which should be distinguished from the systematic, pronounced negative values as shown in the standard protocol (arrows).

Figure 2-3a shows the location of the negative-CVR voxels (corrected $P<0.01$) when using the standard protocol. As expected they are

predominantly clustered in ventricular regions. No such clusters were detected when using the Opt1 or Opt2 protocols. Figure 2-3b shows the CVR values in ventricular region for three protocols. The CVR value for Old protocol in these regions were found to be -0.11±0.02 %BOLD/mmHg CO2. We also applied the negative mask derived from the standard protocol data on the Opt1 and Opt2 data. It was found that the CVR values were -0.02±0.01 %BOLD/mmHg CO2 and 0±0.01 %BOLD/mmHg CO2 for Opt1 and Opt2, respectively, suggesting that the negative artifact is substantially mitigated with the optimized protocols. The Opt1 showed a small negative value, which may be due to imperfection in the assumed parameters in the simulation.

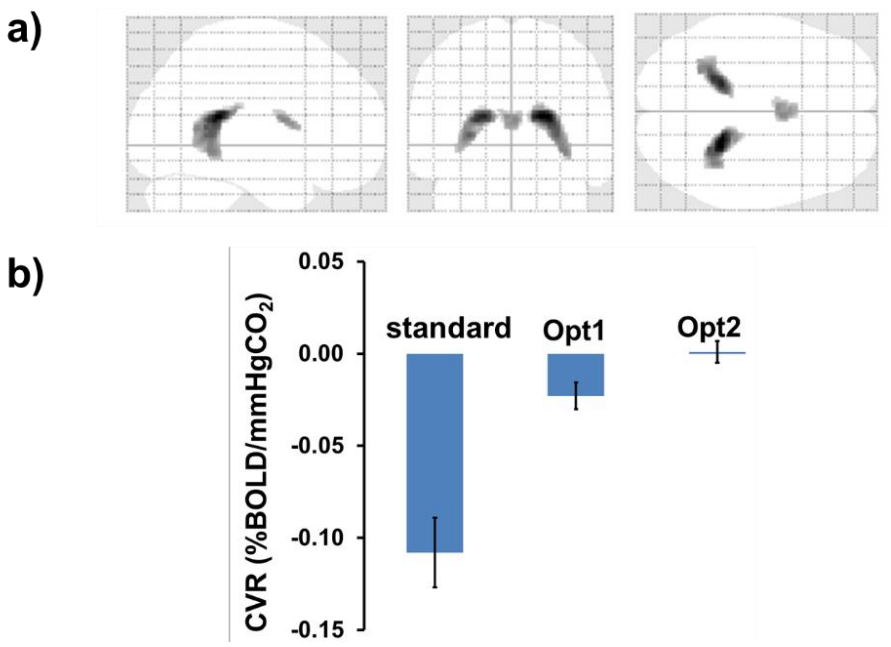

Figure 2-3 Summary of ROI analysis in the ventricular region. (a) The location of negative CVR voxels when using the standard protocol (FWE corrected $p<0.01$). Note that the negative CVR voxels are predominantly located in the ventricular region. When applying the same algorithm to Opt1 and Opt2 protocols, no such clusters were detected. (b) The mask generated in the above step was applied on three protocols individually and CVR values were generated for ventricular region. Note that in Opt1 and Opt2 the negative CVR values are attenuated. The error bar represent standard error of mean (SEM)

We then performed quantitative analysis of CVR results in the brain parenchyma to compare sensitivity across protocols. The bar plots in Figure 2-4a depict the whole-brain CVR values for the three protocols. The CVR

value for the standard protocol (0.21±0.01 %BOLD/mmHg CO2) was significantly ($p<0.001$) greater than that of Opt1 (0.16±0.01 %BOLD/mmHg CO2) and Opt2 (0.15±0.01 %BOLD/mmHg CO2). There was no difference between Opt1 and Opt2. This pattern is expected because CVR is related to BOLD percentage signal change, and the BOLD change is approximately proportional to TE, which is longer in the standard protocol. However, the overall sensitivity of the CVR technique is also related to SNR of individual images, which are shown in Figure 2-4b. The SNR for the standard protocol was found to be significantly lower than both Opt1 ($p=0.003$) and Opt2 ($p=0.013$). The lower SNR in the standard protocol is presumably due to the longer TE used. The results for CNR (i.e. overall sensitivity) are shown in Figure 2-4c. CNR of Opt1 and Opt2 were not different from that of the standard protocol ($p=0.1$). Another means to evaluate the overall sensitivity of a technique is to examine its COV across repetitions. The COV (i.e. a measure of reproducibility) for the three protocols are shown in Figure 2-4d. There were no significant differences across the three protocols ($p=0.65$). We also calculated the COV of individual lobes (frontal, occipital, parietal and temporal) and found no differences across protocol

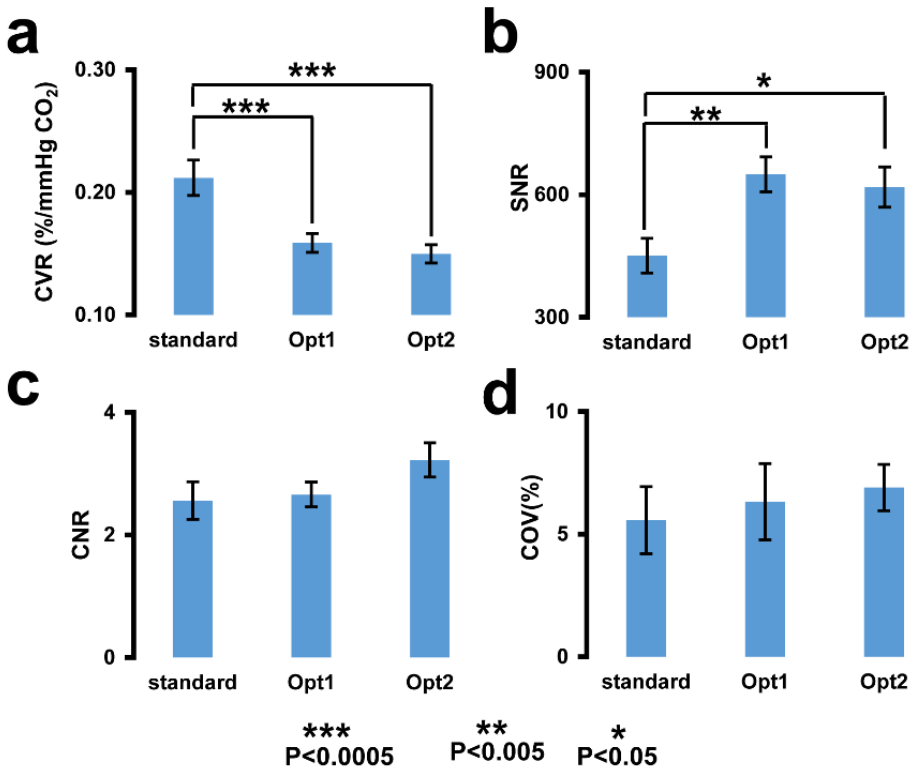

Figure 2-4 Results of quantitative analysis in the whole brain ROI. (a) CVR. (b) SNR per BOLD image. (c) CNR per unit time. (d) Coefficient of variation (COV) across repetitions. The data are presented as mean ± standard error (***: p<0.0005, **: p<0.005 and *: p<0.05).

2.4 Discussion

In this study, we conducted theoretical and experimental investigations to optimize BOLD imaging parameters for the removal of artifactually negative CVR signals while preserving the sensitivity of desired signals. We showed that, when the signal intensities in CSF and blood

compartment are equated, the artifactually negative CVR can be minimized. We have further shown that CNR and reproducibility of the CVR results when using the optimized protocols are comparable to those using the standard protocol. Overall, we recommend the use of a TE shorter than that typically used in fMRI for CVR mapping.

Negative CVR has been noted in a number of studies (Blockley et al., 2011; Conklin et al., 2010; Mandell et al., 2008; Mikulis et al., 2005; Poublanc et al., 2013). Some of them can be attributed to a vascular stealing phenomenon (Poublanc et al., 2013). However, others, especially those in and around posterior horns of the ventricles where the choroid plexus is located, may be due to the artifact described in this study. Therefore, the use of an “artifact-free” BOLD protocol may simply the interpretation of such results. Comparing BOLD images from the three protocols, the standard protocol showed brighter CSF signal than the brain parenchyma, which is consistent with the previous findings (Thomas et al., 2013). In contrast, this difference is clearly attenuated in the Opt1 and Opt2 images, consistent with the simulation criteria. In accordance with these differences in the raw images, the CVR map using the standard protocol showed clearly discernable negative CVR voxels in the CSF regions, although not all voxels with bright CSF signal in Figure 2-2a showed negative CVR because choroid plexus is known to be absent in certain part

(e.g. anterior horns(Waxman, 2009)) of the ventricle. The negative voxels are absent in the Opt 1 and Opt2 results. These data suggest that the intensity differences between CSF and parenchyma in combination with changes in CSF partial volume is the source of negative CVR, and this artifact could be removed with an imaging protocol that equates CSF and parenchymal signals. Note that this principle also applies to parenchymal voxels, should CSF partial volume in those voxels be replaced by blood partial volume. But it is expected that the size of the effect may be smaller in typical parenchyma voxels.

The CVR values obtained from the Opt1 and Opt2 protocols were considerably lower than that from the standard protocol. This is expected considering their different TE values. Therefore, when comparing reported CVR values across studies or protocols, it is important to evaluate them in the context of the TE used. Shorter TE is known to result in lower CVR values. In terms of sensitivity, the lower CVR values in the Opt protocols appear to be offset by a higher SNR, and consequently the overall CNR was comparable among the protocols tested. Comparing the two optimal protocols with different TR values, theoretical estimation (Figure 2-1d) and experimental CNR (Figure 2-4c) suggested that the shorter TR one (i.e. Opt2) should yield a higher sensitivity, owing to the greater number of images per unit scan time, which is helpful in boosting the overall CNR

(Equations [4] and [5]). However, the CoV result, which is another indicator of sensitivity, revealed (Figure 2-4d) that Opt2 is slightly less sensitive, although the difference was not significant due to small sample size. This discrepancy could be because Equations [4] and [5] assumed that the image series are temporally independent, whereas in reality the noise may be partially correlated. Thus, CNR of Opt2 in Figure 2-4c and simulations may be slightly over-estimated.

We also evaluated the COV (reproducibility) of the three protocols. The COV values in our experiment were less than 7%. Compared to COV values reported in the literature, e.g. 26% in (Goode et al., 2009), 8% in (Lipp et al., 2015), and 8.8% in (Tancredi et al., 2015), the values in our study for all the protocols were comparatively lower. This suggests that irrespective of BOLD protocol used in this study for measurement of CVR, the experimental design and data analysis used in our experiment is quite reproducible. The COV showed subtle variation across the three protocols tested. However, there were no significant differences among them. We also evaluated COV in the four major lobes (frontal, parietal, occipital, and temporal) of the brain. The findings were similar. Low COV (i.e. high reproducibility) enhances the potential of an imaging tool to find utility in clinical settings.

The clinical importance of the proposed optimal protocol is that it

minimizes artifactually negative CVR signals, thereby improving the specificity of pathological indications of negative CVR. Negative CVR has been previously reported in patients with cerebrovascular diseases as evidence of a loss of vascular reserve (Fierstra et al., 2011b; Mikulis et al., 2005). However, the potential of artifactual signal source could cloud the interpretation of such results. Therefore, the optimized BOLD protocol could remove the “volume effect” and ascertain the correct identification of vascular stealing territory in patients with, for example, arterial stenosis.

The primary limitations of this study are the use of only young healthy participants and the relatively small sample size. Our participants have an average age of 29 years thus do not represent typical patients seen in clinical settings. Therefore, a study in elderly individuals with no known pathology would be useful in future investigations. Also, our sample size of 10, is modest. Even though we were able to show significant group-averaged results and an estimation of reproducibility, the lack of significant difference in some comparisons, e.g. CNR across protocol, could be due to insufficient power. Thus, future studies are needed to verify our findings. In conclusion, an optimized BOLD imaging protocol was devised that allows the removal of negative signal artifacts in CVR mapping. The optimal protocol yields a sensitivity and reproducibility comparable to that of a standard protocol. To our knowledge, this is the first report to investigate

the BOLD optimization for CVR mapping. We showed that, when the signal intensities in CSF and blood compartment are equated, the artifactually negative CVR can be minimized. We have further shown that CNR and reproducibility of the CVR results when using the optimized protocols are comparable to those using the standard protocol. Overall, we recommend the use of a TE of 20-23 ms for BOLD-based CVR mapping, as opposed to the 30-40 ms range commonly used in brain activation fMRI studies. The availability of such a protocol may improve the interpretability of CVR results in clinical settings.

Chapter 3

Multiband BOLD acquisition enhances the sensitivity of cerebrovascular reactivity (CVR) mapping

3.1 Introduction

Cerebrovascular reactivity (CVR) represents the dilation capacity of the arterial vasculature to a vasoactive stimulus. CVR is used as stress test to assess the integrity and functionality of the cerebral vasculature (Thomas et al., 2013; Yezhuvath et al., 2009a). Furthermore, It has been used to assess and evaluate many cerebral and cerebrovascular pathologies (Glodzik et al., 2013; Greenberg, 2006a; Han et al., 2008; Mandell et al., 2008b; Mikulis et al., 2005; Yezhuvath et al., 2012; Zhao et al., 2007), to study the effects of drugs on cerebral vasculature (Pattinson et al., 2007; St Lawrence et al., 2002) and also presurgical planning (Zaca et al., 2011a).

BOLD MRI based measurement technique is most commonly used technique for measuring CVR, in this technique a physiological maneuver is applied to alter the arterial gas concentration, while continuously measuring perfusion sensitive BOLD MR images (Gauthier et al., 2012; Kastrup et al., 2001; Rostrup et al., 2000; Thomas et al., 2013; Yezhuvath et al., 2009b). However, like other functional and physiological indices, the biggest drawback of BOLD technique is its poor sensitivity and reliability (de Zwart et al., 2008). Signal changes measured during gas inhalation

challenge amounts only a small fraction (~1-3%) of the total BOLD signal. Furthermore, the ability to detect these small BOLD signal changes from time-series data is confounded by the presence of various noise sources, including thermal and non-thermal noise, head motion, and physiological fluctuations (e.g., cardiac and respiratory cycles).

Most commonly used strategies to improve the sensitivity are 1) averaging across multiple scans to reduce the effects of noise and 2) scanning for longer time to increase the statistical power (Murphy et al., 2007; Saad et al., 2003). However, both the above discussed strategies would lead to subject staying in the scanner for longer time performing breathing challenges, thereby increasing subject discomfort. Alternatively, faster acquisition rate (i.e. shorter TR) has been hypothesized to provide sensitivity improvement similar to long scan time (Henson, 2005; Posse et al., 2012). However, the faster acquisition rate comes with a price of lower brain coverage.

Recently, multiband echo planar imaging (EPI) demonstrated the capability of acquiring whole brain coverage with lower TR i.e. higher temporal sampling rate (Feinberg et al., 2010). Multiband EPI is a fast-imaging technology that allows the excitation and acquisition of multiple 2D slices simultaneously (Setsompop et al., 2012). Multiband EPI feasibility and sensitivity improvement over convention EPI has been already shown

in fmri and DTI applications (Feinberg et al., 2010). To our knowledge, the use of multiband acquisition for CVR mapping has not yet been investigated.

In this work, we examined the sensitivity benefit of multiband acquisition in CVR mapping, by comparing the data collected using multiband 2 (MB2) and multiband 3 (MB3) with those using conventional EPI (MB1). Furthermore, we also investigated the influence of resolution changes and scan time reduction on the CVR.

3.2 Methods

The study was approved by the Institutional Review Board of the University of Texas Southwestern Medical Center. All subjects gave informed written consent before participation. All experiments were performed on a 3T (Philips) system using 32 channel head coil. Five healthy volunteers (Age 30±4 years) were scanned for this study.

3.2.1 Experimental Procedure

We used two spatial resolutions, standard-resolution (3.2x3.2x3.5 mm^3) and high-resolution (2.5x2.5x3 mm^3) in this study. We acquired three different multiband factors, MB1 (conventional EPI), MB2 (2 slices excited and acquired at a time), and MB3 (3 slices excited and acquired at a time) for each resolution, resulting in a total of six scans on each participant.

We used simultaneous hypercapnia and hyperoxia protocol in this

study, which was implemented previously (Liu et al., 2014). The experimental setup used in this study is shown in Figure 3-1a). Subject was fitted with a nose clip and a mouthpiece to allow breathing through the mouth. The end of the mouthpiece is connected to five way valve which is again connected to three Douglas bags containing different gas mixture. During the respiratory challenge, EtCO2 was recorded using a capnograph device (Capnogard, Model 1265, Novametrix Medical Systems, Wallingford**,** CT, USA) and EtO2 was recorded using an O_2 monitoring device (Biopac system,Goleta,CA,USA). The gas inhalation paradigm used in this study is shown in Figure 3-1b). Briefly, the timing of the CO_2 and O_2 paradigm were carefully designed so that they are orthogonal to each other in the time domain and have different frequencies in the frequency domain. BOLD signal change to CO_2 would result in CVR; and BOLD signal change to O_2 gives O_2-reactivity which reflects venous CBV (vCBV). The composition of gases used in this study are hypercapnia (5% CO_2, 21% O, and 74% N_2), hyperoxia (95% O_2, and 5% N_2) and carbogen (95% O_2, and 5% CO_2) when there is an overlap in both paradigms. During each scan, the participant underwent a simultaneous hypercapnia and hyperoxia respiratory task lasting for 9.3 minutes.

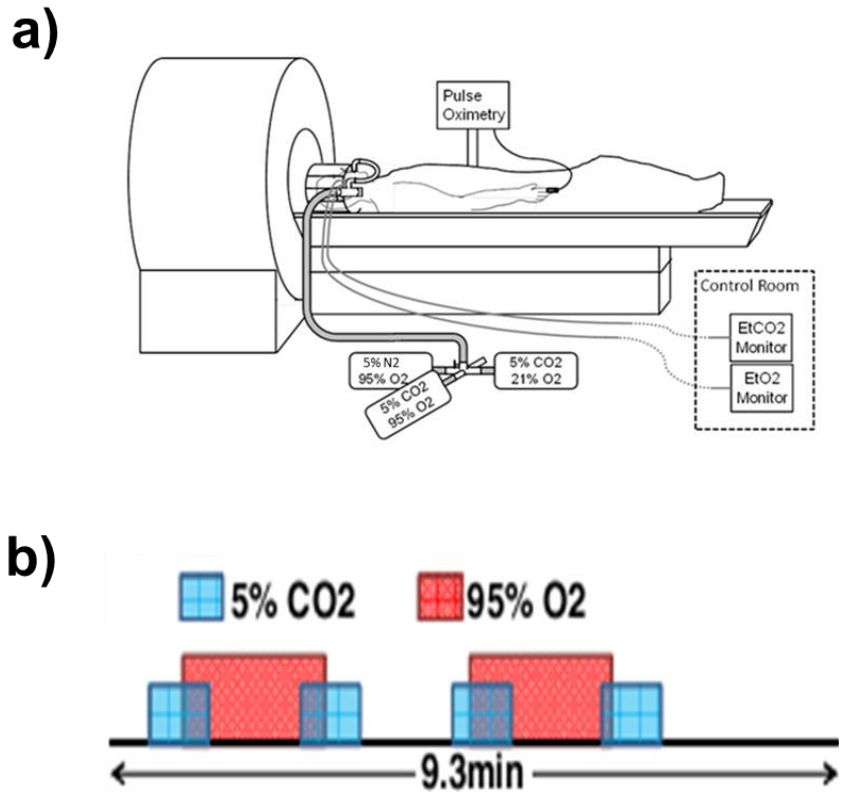

Figure 3-1 A graphical illustration simultaneous hyperoxia and hypercapnia experimental design. a) Experimental setup used in this study is shown in the top row, the subject is fitted with a nose clip and mouthpiece to facilitate breathing through the mouth. The mouthpiece is connected to a long tube and the end of this long tube is connected to different gases using a five way valve. Simultaneous EtCO2 and EtO2 is recorded using capnogard and biopac system respectively. b) The paradigm used in this study is shown in the bottom row. It consists of both hypercapnia and hyperoxia breathing challenges. The timing of both these challenges is selected such that they are orthogonal to each other in time domain and have different frequency in the frequency domain.

The order of the three protocols was randomized for each subject. The participant was allowed to come out of the scanner after each resolution session and took a break before entering it again. The TE for the BOLD imaging protocols were optimized to remove artifactual negative CVR (Ravi et al., 2015). The scan parameters used in this study are listed in Table 3-1.

Table 3-1 Summary of the imaging parameters used in this study.

Standard	MB1	MB2	MB3
vox=3.2x3.2x3.5 mm^3, mat=64x64x36,SENSE=2 ,FA=90^0, FOV=205x205, Slice number=36.	TR=1550 ms	TR=900 ms	TR=650 ms
	TE=21 ms	TE=25 ms	TE=27 ms
	Dynamics=362	Dynamics=624	Dynamics=862
High	**MB1**	**MB2**	**MB3**
vox=2.5x2.5x3 mm^3, mat=84x80x42,SENSE=2, FA=90^0, FOV=205x205, Slice number=42.	TR=1950 ms	TR=1100 ms	TR=850 ms
	TE=19 ms	TE=24 ms	TE=26 ms
	Dynamics=288	Dynamics=510	Dynamics=660

3.2.2 Data analysis

The Statistical Parametric Mapping (SPM) software, (University College London, UK) and in-house MATLAB (MathWorks, Natick, MA) scripts were used for the processing of BOLD data. Pre-processing included realignment of BOLD images, normalization to Montreal-Neurological-

Institute (MNI) template space with a resolution of 2x2x2 mm^3, and finally smoothing using a 6mm full width half maximum (FWHM) Gaussian kernel.

For each subject, a General Linear Model (GLM) was used to calculate voxel-by-voxel CVR in units of % BOLD signal change per mmHg CO_2 and O2-reactivity in units of %BOLD signal change per mmHg O_2. To evaluate the impact of reducing scan time on vascular reactivity measurements, the BOLD timeseries was divided into 2 halves and were labeled first half and second half. Both half data sets were again used to generate respective CVR and O2-reactivity measures and sensitivity estimates. Additionally, intraclass correlation (ICC) coefficient was also calculated, which tests the consistency of the spatial distribution between the halves, for both the vascular reactivity maps. The ICC described previously (Caceres et al., 2009) was used in this study.

3.2.3 Statistical analysis

We compared the histogram distribution of the Z scores for conventional EPI scans and multiband scans. Student t test was also performed in this study and a p-value less than 0.05 was considered significant. Furthermore, a voxel by voxel paired t test was also performed on Z score maps. The paired ttest was performed to visualize and quantify the extent of whole brain sensitivity improvement. Voxels showing t score greater 3 were considered significant.

3.3 Results

We first performed a visual inspection on vascular reactivity maps. Figure 3-2a shows CVR maps of a representative subject, the top row represents standard resolution and bottom row represent high resolution scans. Qualitatively, similar gray to white contrast was observed in the conventional EPI scan (MB1) and multiband (MB2 & MB3) scans. Figure 3-2b show the O2-reactivity maps. Again, it can be observed that, almost identical gray to white contrast was observed across both resolution for O2-reactivity maps. Quantitative ROI analysis was then performed to generate the whole brain vascular reactivity values. The CVR values for “MB1”, “MB2” and “MB3” protocols were 0.19±0.01, 0.21±0.02 and 0.22±0.01 for standard- resolution, and 0.15±0.02, 0.19±0.02, and 0.21±0.02 %/mmHg for high resolution scans. The higher CVR in multiband protocols is due to longer TE used in these protocols. The summary of vascular reactivity measures is given in Table 3-2. However, greater vascular reactivity measures do not necessarily indicate higher statistical significance (sensitivity). We therefore examined the Z scores associated with these maps.

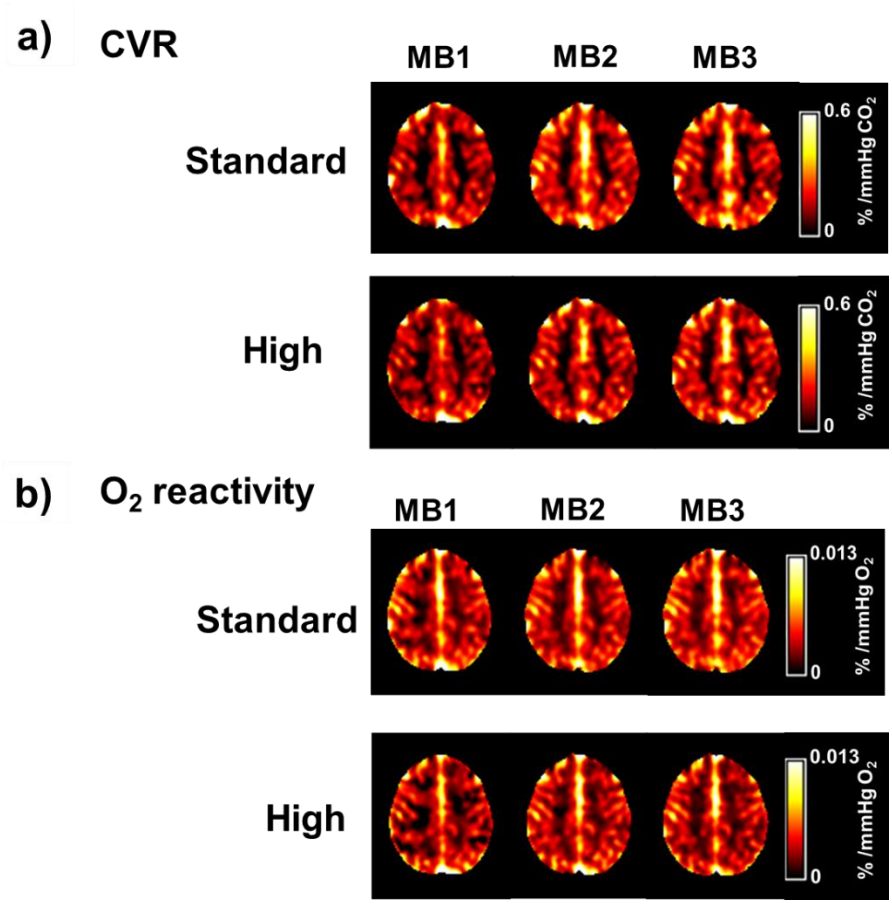

Figure 3-2 CVR and O2-reactivity maps from a representative subject. a) CVR maps. b) O2-reactivity maps. Note, the top row represents a standard resolution and bottom row represent high resolution scans in both a) and b). The images from left to right represents vascular reactivity maps for MB1, MB2 and MB3 respectively.

Table 3-2 Summary whole brain of vascular reactivity measures for conventional EPI scan and multiband scans (mean ± SEM).

Resolution	CVR (%/mmHg CO_2)			O2-reactivity (%/mmHg O_2)		
	MB1	**MB2**	**MB3**	**MB1**	**MB2**	**MB3**
Standard	0.19±0.01	0.21±0.02	0.22±0.01	0.0048±0.01	0.0049±0.02	0.0052±0.03
High	0.15±0.02	0.19±0.02	0.21±0.01	0.0042±0.01	0.0046±0.02	0.0048±0.02

Figure 3-3 shows a comparison of Z score histograms for each of the map types, i.e. (a) standard-resolution CVR, (b) high-resolution CVR, (c) standard-resolution O_2-reactivity and (d) high-resolution O_2-reactivity. The black histogram represents MB1 protocol, and blue and red histogram represent MB2 and MB3 protocols respectively. It can be observed that, the distribution center of MB2 and MB3 is at a higher Z score value compared to MB1. The summary of whole brain region of interest (ROI) Z scores is given in the table 3. The Z score of multiband scans ($p<0.005$) were significantly higher than conventional EPI scans. There was no significant difference between MB2 and MB3. This data suggests that multiband acquisition yields statistically more significant data compared to conventional EPI scan due to faster acquisition rate.

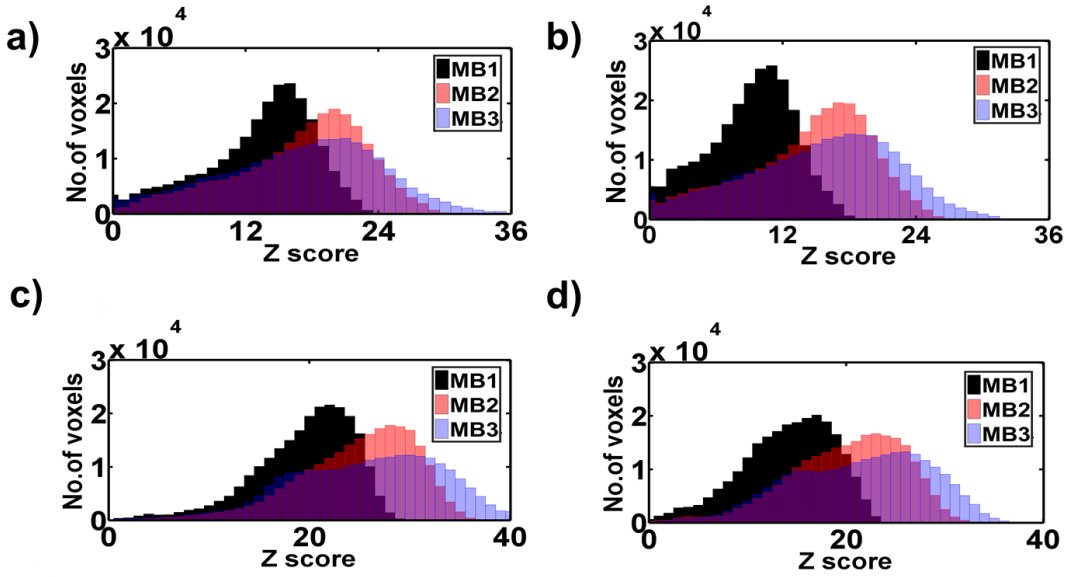

Figure 3-3 Average Z score histograms. (a) Standard-resolution CVR map, (b) High-resolution CVR map, (c) Standard-resolution O2-reactivity map, and (d) High-resolution O2-reactivity map. Note that the black, blue, and red represents MB1, MB2 and MB3 Z score histograms respectively.

Table 3-3 Summary whole brain average Z scores of vascular reactivity measures (mean ± SEM).

Resolution	**CVR (%/mmHg CO_2)**			**O2-reactivity (%/100mmHg O_2)**		
	MB1	**MB2**	**MB3**	**MB1**	**MB2**	**MB3**
Standard	13±1.0	17±1	17±1	20±1	25±1	26±1
High	9±1	15±1	16±1	14±1	21±1	22±1

Figure 3-4 shows the bar plots of whole brain ROI Z score for CVR (Figure 3-4a) and O_2-reactivity (Figure 3-4b). In the Figure 3-4 the blue standard and orange bar plot represent standard and high resolution scan respectively. It can be observed that for both CVR and O2-reactivity, standard-resolution scans showed higher mean Z score value compared to high-resolution scans, indicating a better sensitivity for standard resolution scans. The relative reduction (from standard to high resolution) in Z score

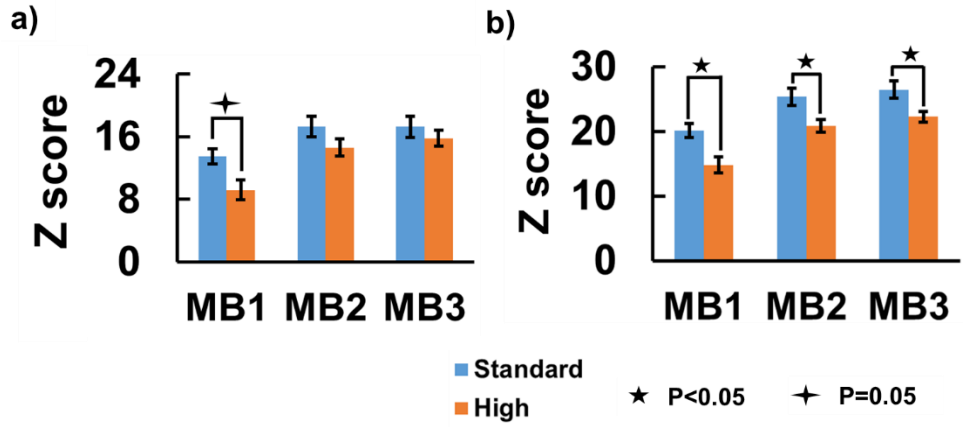

Figure 3-4 Comparisons of Z scores between standard-resolution and high resolution scans. a) CVR comparisons. b) O2-reactivity comparisons. The blue bar plot represents standard reolsution scan and red represents high resolution scans.

was on an average 31 % for MB1 data, on the other hand the observed reduction was 14% and 6 % in MB2 and MB3 data respectively. For O_2-reactivity, similar pattern was observed in Z scores changes, where

standard resolution showed higher Z score values compared to high resolution scans and these differences were statistically significant ($P<0.05$), and the relative reduction of Z score was 27 %,18 % and 16% for MB1, MB2 and MB3 respectively.

We further compared the sensitivity between CVR and O_2-reactivity. Comparing the Z scores between CVR and O_2-reactivity across multiband factors and scan resolutions, it was found that the Z scores of the O_2-reactivity was significantly higher ($p<0.005$) than CVR. This would indicate an over-all higher sensitivity of O_2-reactivity than CVR.

Figure 3-5 shows t score distribution map for voxel by voxel comparison of Z score between multiband scans and conventional EPI scan. The dashed line in the figure represents the statistical threshold (t score =3) and a voxel which shows t score greater than this threshold is considered to be significant. When directly contrasting MB2 to MB1 (Figure 3-5a, top row) data in a voxel-by-voxel comparison, it was found that 28% of the voxels in the brain showed a greater Z score in the MB2 data. When comparing MB3 to MB1 (Figure 3-5a, bottom row), this fraction was 20%. In the case of high-resolution scan, 45% of total voxels in MB2 (Figure 3-5b, top row) and 38% (Figure 3-5b, bottom row) of total voxel in MB3 showed higher Z score voxels than MB1. No apparent difference was observed between MB2 and MB3, suggesting that further sensitivity

increase might not be possible when going to a higher MB factor. Similar observations can be made for O_2-reactivity data. A summary of the percentage of whole brain voxels in multiband scans showing higher Z scores when compared to conventional EPI is given in Table 3-4.

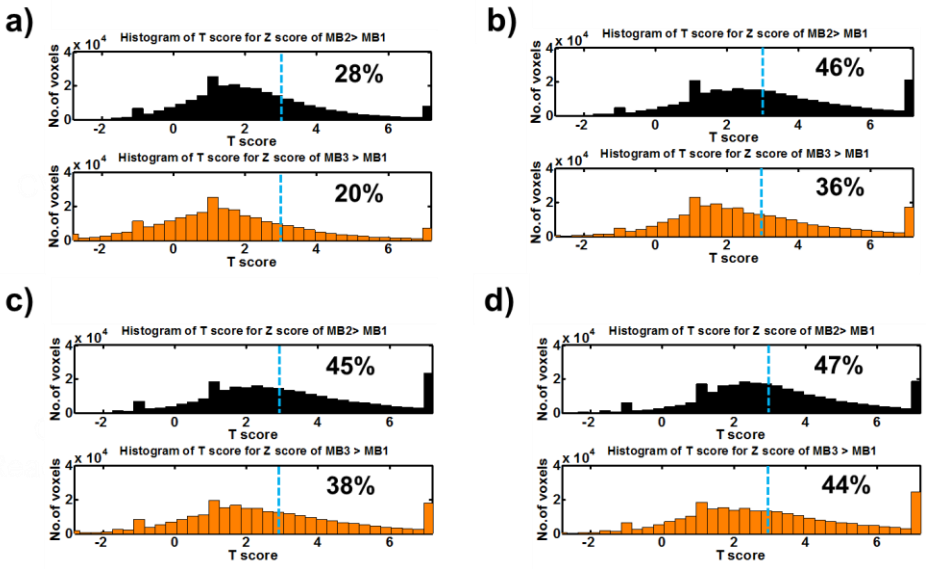

Figure 3-5 T score histograms for Z scores comparison between conventional EPI (MB1) and multiband (MB2&MB3) scans. a) Comparison Z scores for standard-resolution CVR map, b) Comparison Z scores for High-resolution CVR map, c) Comparison Z scores for Standard-resolution O2-reactivity map, and d) Comparison Z scores for High-resolution O2-reactivity map. Note that the upper row for each of these figures represent histogram of T scores for Z score comparison of MB2>MB1 and bottom row represent histogram of T scores for Z score comparison of MB3>MB1.

Table 3-4 Summary percentage voxels in multiband scans which show statistically significant higher sensitivity compared to conventional EPI scans.

Resolution	CVR (%)		O2-reactivity (%)	
	MB1 vs MB2	MB1 vs MB3	MB1 vs MB2	MB1 vs.MB3
Standard	28	20	45	38
High	46	36	47	44

Shown in Figure 3-6, vascular reactivity maps generated using full, first half, and second half data set for standard resolution. CVR maps are shown in Figure 3-6a) and O2-reactivity maps are in Figure 3-6b). Visual inspection of CVR maps generated from half data set show similar gray to white contrast as that of CVR maps generated using full data set. Comparing the quantitative CVR and O2-reactivity values for full data and both half data no significant difference was observed.

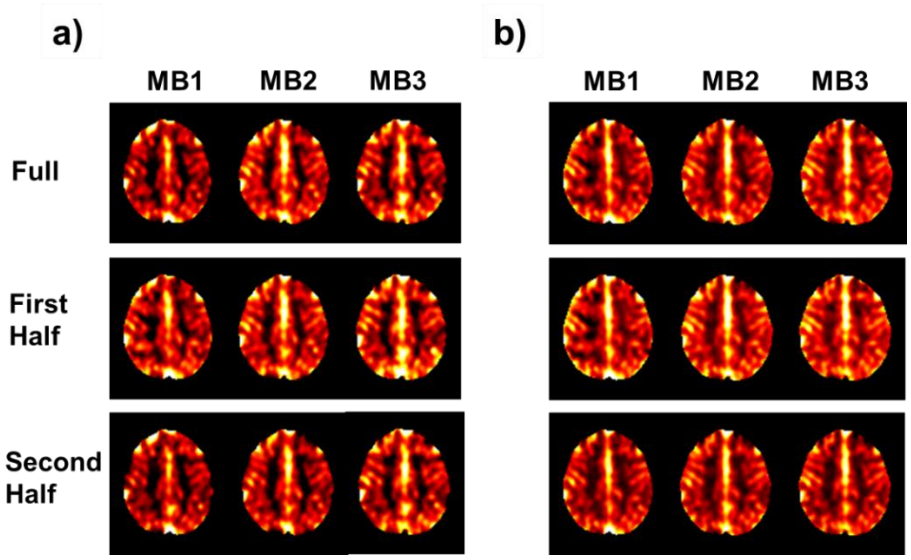

Figure 3-6 CVR and O2-reactivity maps for standard resolution scan from a representative subject for full data, first half data, and second half data. a) CVR maps. b) O2-reactivity maps.

The results ICC is shown in Figure 3-7. The ICC values were greater than 0.9 for all the scans, any value greater than 0.8 is taught to result in excellent reproducibility (Li et al., 2015; Oremus et al., 2012). This data suggests that the CVR and O2-reactivity maps generated from first half and second half data set would have similar spatial distribution pattern.

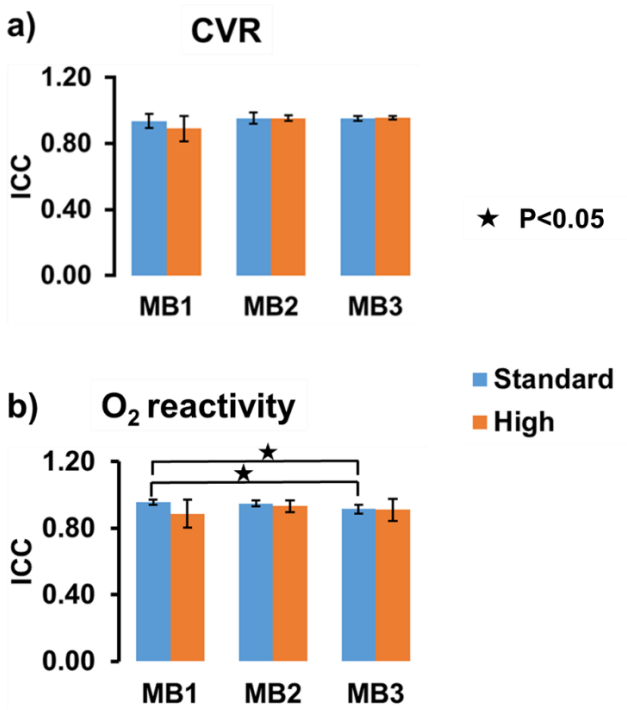

Figure 3-7 Bar plot for ICC values across all resolution scans. a) CVR and b) O_2-reactivity. The blue color plot represent standard resolution and orange color represents high resolution scan. The ICC values close 0.9 for most of the scans.

We further analyzed the Z score of all the data sets. Shown in Figure 3-8 are Z scores plots for all the data sets i.e. (a) standard-resolution CVR, (b) high-resolution CVR, (c) standard-resolution O2-reactivity and (d) high-resolution O2-reactivity. The blue, orange and gray plots represent Z scores for full, first half and second half data sets respectively. It can be observed that the full data set Z scores are consistently greater than Z scores of the first half and second half data set across all the scans. This is expected due

to reduced number of data points in both half data sets. Interestingly, when Z score of the full data set (indicated in a dashed line) MB1 (conventional EPI scan) compared with a Z score of both half data sets of MB2 & MB3 (multiband scans), either no difference or smaller Z score was observed for conventional EPI scan. This would indicate that the sensitivity of multiband scans is similar to that of conventional EPI scans with double the scan time.

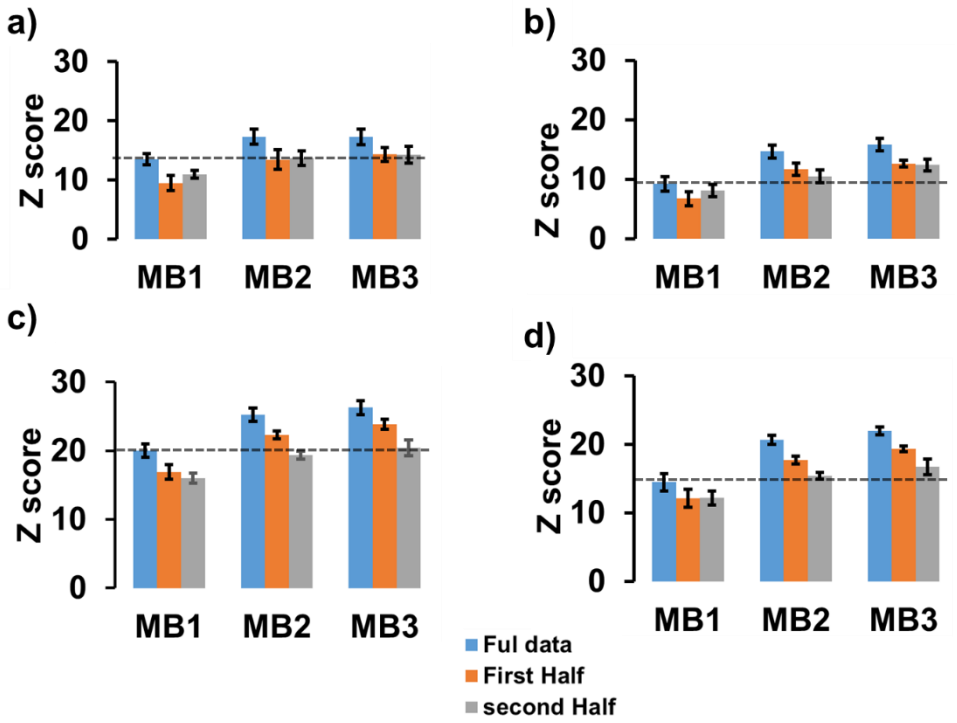

Figure 3-8 Average Z score. (a) Standard-resolution CVR, (b) High-resolution CVR, c) Standard-resolution O2-reactivity, and d) High-resolution O2-reactivity. Note that the Z score of full, first half and second half data set is represented in blue, orange, and gray respectively. The dashed line indicate the Z score level of MB1 for full data set. Note that the Z score generated using first half and second half data set in the multiband scans (MB2&MB3) showed similar or a trend of higher Z score values when compared to Z score values of conventional EPI scans generated using full data set.

3.4 Discussion

BOLD based vascular reactivity measurement is most commonly used technique. However, BOLD based measurement suffer from low sensitivity due to inherently small signal changes observed during gas inhalation challenges. The detection sensitivity is further confounded by the presence of noise sources. To extract meaningful information from these small signal changes during BOLD experiments we need a sensitive technique. In this study we showed the feasibility and superiority (in sensitivity) of the multiband acquisition for vascular reactivity measurements. To our knowledge this is the first report to investigate the advantage of using multiband acquisition for measuring the vascular reactivity measures. We further found that the relative reduction in sensitivity when moving from standard resolution scan to high resolution scan was less in the multiband acquired data. Furthermore, we also observed that scan time is directly related to sensitivity and reducing the scan time would lead to loss in sensitivity. Interestingly, we found that the multiband scans provide sensitivity similar to the conventional EPI scans with double the scan time.

The visual inspection of both CVR and O2-reactivity maps showed similar gray to white contrast across multiband and conventional EPI scans, asserting the qualitative similarity across the scans. The quantitative

analysis showed higher CVR and O2-reactivity values in multiband scans compared to conventional EPI scans due to longer TE used in multiband scans. It can be argued that higher effect size in multiband scans could lead to higher sensitivity, however, the lower signal-to-noise ratio (SNR) due to shorter TR and longer TE could potentially counteract this sensitivity gain. Therefore, higher vascular reactivity values do not always indicate higher sensitivity. Thus, we investigated the Z score, which indicates statistically sensitivity of a measurement technique.

Comparing Histogram of Z scores for conventional EPI with the multiband scans, it was observed that the distribution center of multiband scans was at a higher Z score value compared to the convention EPI scans. Moreover, voxel by voxel comparison of Z scores also revealed that the multiband scans showed sensitivity improvement across the whole brain compared to conventional EPI scans. The percentage of voxels in whole brain which showed sensitivity improvement for multiband scans ranged from 20% to 48% across all the scans. The power of a statistical inference is directly related to the number of independent degrees of freedom (df), and the df depends on the number of scans (Henson, 2005). The multiband scans in this study yielded a higher number of total time points compared to conventional EPI scans and this could have potentially boosted the statistical power of the multiband scans. However, when we compared the

Z score between MB2 and MB3, no significant difference was observed. This may be related to temporal autocorrelation of the sample data. In general, the effective df depends on temporal autocorrelation of sampled data i.e 862 scans acquired in MB3 doesn't mean 862 independent observations. So there may be a limit to the statistical power increase afforded by reducing TR (Henson, 2005). Overall, the multiband scans show improved sensitivity compared to conventional EPI scans. This additional sensitivity gained through multiband acquisition could be used to either acquire higher spatial resolution data or to reduce the scan time. Therefore, we further investigated the sensitivity changes in vascular reactivity estimates due to high resolution scans and also reduce scan time.

We first compared the Z scores between standard and high resolution scans, it was observed that the standard resolution scans showed a trend of higher Z score values compared to high resolution scans. This reduced sensitivity in high resolution scans could be due to low SNR in high resolution scans. However, compared to conventional EPI scans, the multiband scans showed smaller decrease in sensitivity from standard resolution to high resolution scans. This result suggested that the high resolution scans could benefit more from the application of multiband acquisition.

Since it is commonly suggested that the higher statistical power

garnered in multiband scans could be due to increase in number of data points in the acquired data set. We tried to tease out the influence of data size alone on sensitivity. Therefore, the whole data set was truncated into two equal halves and the vascular reactivity and sensitivity measures were again generated from this truncated data. The changes in vascular reactivity and sensitivity of truncated data were evaluated. The qualitative vascular reactivity values and quantitative CVR values did not show any difference. As expected, the truncated data showed lower sensitivity compared to full data due to reduce number of data points (i.e df). This result again ascertains the hypothesis that higher degrees of freedom could potentially lead to higher sensitivity. Interestingly, the Z scores of truncated data set in the multiband scans showed either increase or no difference in sensitivity when compared with Z scores of full data set for conventional EPI scans. This may be due to similar degrees of freedom between truncated data set in multiband scans and full data set in conventional EPI. This result suggest that we can reduce the scan time of a CVR protocol where sensitivity not a constraint.

The O2-reactivity value was approximately 4 times lower than the CVR. However, the Z scores of O2-reactivity were higher compared to CVR across all scans. This may be due to higher SNR in BOLD response to hyperoxia challenge (Bulte et al., 2009).

In clinical practice, the use of vascular reactivity mapping is gaining a lot interest. Especially CVR mapping and O2-reactivity mapping has been recently used for understanding the effects of pharmacological agents on cerebrovasculature (Pattinson et al., 2007; St Lawrence et al., 2002), presurgical planning (Zaca et al., 2011a) and understanding the pathophysiology of pathological conditions (Johnston et al., 2003). Therefore, the higher sensitivity achieved by multiband acquisition in CVR and O2-reactivity mapping might benefit a large range of clinical applications and could also open doors for use CVR in unexplored research territories. Additionally, a sensitive technique could provide accurate detection of physiologic changes at individual subject level and could play an important role as a routine diagnostic tool for pre-surgical, where individual differences in brain function are crucial.

The major caveat of this study is a small sample size. The use of small sample size might be one of the reasons behind some of the observed difference for not being significant. Another caveat of this study is signal leakage between simultaneously excited slices. It has been recently reported that multiband acquisition leads to signal leakage and this signal leakage scale with the multiband factor. The signal leakage may lead to noisy reconstruction (Preibisch et al., 2015; Todd et al., 2016; Xu et al., 2013). The additional noise introduced at higher acceleration factor may be

one of the reasons for not observing sensitivity improvement in MB3 scans when compared MB2 (Todd et al., 2016).

We have shown the successful use of multiband in CVR mapping. We also showed that the sensitivity of MB scans was higher compared to conventional EPI scans owing to faster data acquisition rate. Additionally, we found that multiband acquisition is less susceptible to resolution changes, suggesting that higher resolution scans could benefit more from the use of multiband acquisition. Furthermore, we showed that if sensitivity is not a confounding factor for an application, we can reduce the scan time using multiband scans. The availability of a sensitive technique would further encourage clinicians to adopt the use of CVR for future clinical applications.

Chapter 4

An investigation on nonlinearity in BOLD response during moderate hypercapnia challenge

4.1 Introduction

Cerebrovascular reactivity (CVR) refers to the change in cerebral blood flow (CBF) response to a vasoactive stimulus (Kety and Schmidt, 1948). CVR has many clinical implications and application. Impaired CVR has been linked to many cerebral and cerebrovascular pathologies (Glodzik et al., 2013; Greenberg, 2006a; Han et al., 2008; Mandell et al., 2008b; Mikulis et al., 2005; Yezhuvath et al., 2012; Zhao et al., 2007), and also been studied in connection with dementia (Gupta et al., 2012; Silvestrini et al., 2000), and Alzheimer's disease (Silvestrini et al., 2012; Yezhuvath et al., 2012). Additionally, CVR has also been used to understand effects of pharmacological agents on vascular physiology (Pattinson et al., 2007; St Lawrence et al., 2002), presurgical planning (Zaca et al., 2011a), and to evaluate patient outcome following corrective cerebrovascular surgery (Han et al., 2011). CVR also has implications in calibration fmri (Davis et al., 1998; Gauthier and Hoge, 2013).

In general, a linear regression model (i.e. linear increase in CBF with EtCO2) is used to quantify CVR (Alexander et al., 1964; Grubb et al., 1974). Research exploring the physiological origin of CVR using TCD has

demonstrated a sigmoidal relationship between arterial CO_2 and CBF when a progressive ramp stimulus was used as a vasoactive agent. Recently, Bhogal et. al. observed similar nonlinear changes in BOLD MRI signal during progressive hypercapnia challenge (Bhogal et al., 2014). Despite the complexities associated with the CBF-CO_2 relationship, the clinical studies have used linear regression model to quantify CVR (Battisti-Charbonney et al., 2011; Claassen et al., 2007). A non-linear relationship between BOLD responses to an applied stimulus would complicate the interpretation of clinical BOLD based CVR results. Also, the experiments using progressive ramp stimulus challenge the system to severe hypercapnia. The stimulus used in these studies changes the EtCO2 beyond the normal range used clinical setting which would lead to hyperventilation (Bhogal et al., 2014) and could potentially cause discomfort to the patient. However, the nonlinearity in BOLD response to moderate hypercapnia challenge has not been investigated. So we investigated the non-linearity BOLD response during moderate hypercapnia (5% CO_2) challenge.

The aim of this study was to investigate the non-linearity in BOLD response during a moderate hypercapnia challenge. We proposed an improved modeling scheme that incorporates possible nonlinearity while preserving the linear effect, through which we investigated the extent of

nonlinear effect in CVR data and its dependence on age. Furthermore, we also investigated the age and gender differences in EtCO2 measurements.

4.2 Methods

4.2.1 General

All experiments were performed at 3T (Philips Healthcare, Netherlands) Philips scanner using a body coil for transmission and an eight channel head coil for receiving. The volunteers were all fitted with foam pads to reduce head motion.

4.2.1.1 Participants

The data used in this study was collected previously for the cohort of a large-scale aging study, the Dallas Lifespan Brain Study (DLBS), which is a comprehensive life span study on cognitive function and neuroimaging. The UT Southwestern Institutional Review Board approved the Health Insurance Portability and Accountability Act (HIPAA) compliant protocol and written informed consent was obtained from all participants. Participants were screened for health issues and did not show any contraindications to MRI scanning (pacemaker, implanted metallic objects, and claustrophobia). A total of 207 (Female =125, male=82) subjects were scanned. All participants who were included in the study were generally of good health, with no serious or unstable medical conditions such as neurological disease, brain injury, uncontrollable shaking, past bypass surgery or

chemotherapy, or use of medications that affect cognitive function. A small portion of the subjects reported (Thirty-three subjects) reported a diagnosis of hypertension and were using antihypertensive medications (mostly angiotensin converting enzyme inhibitors, beta-blockers, and angiotensin II receptor antagonists). Most of the hypertensive subjects were older participants.

4.2.1.2 Experimental Design

The BOLD measurement during hypercapnia challenge was performed using a CO_2-inhalation paradigm described previously (Yezhuvath et al., 2009a). The subject was fitted with a nose clip and a mouthpiece to allow mouth breathing. The subject inspired room air and the hypercapnia gas in an interleaved fashion (60 sec room air followed by 60 sec CO_2, repeated three times with additional 60 sec room air inhalation at the end). The subject with sealed nose breathed through a mouthpiece that connected to a 5% CO_2 gas bag or room air. The composition of the hypercapnia gas was 5% CO_2, 74% N_2 and 21% O_2. The type of air inhaled was switched via a valve in a 1min interleaved manner while BOLD images and physiologic parameters (end-tidal CO_2, breathing rate, heart rate, and arterial oxygenation) were continuously collected for 7min. A research assistant was always present in the scanner room during the experiment to monitor the subject and switch the valve that controls the delivery of

hypercapnia gas and room air. End tidal CO_2 (EtCO2) a surrogate for concentration of CO_2 in the arterial blood, was recorded for the entire duration of the scan using a capnograph device (Capnogard, Model 1265, Novametrix Medical Systems, CT). Imaging parameters used in this study were FOV = 220 × 220 mm^2, matrix size = 64 × 64, 43 axial slices, thickness = 3.5 mm, no gap, TR/TE/flip angle = 2000 ms/25ms/80°, single-shot EPI. Additionally, magnetization-prepared rapid acquisition of gradient echo(MPRAGE) sequence, TR/TE/TI = 8.1 ms/3.7 ms/1100 ms, flip angle = 18°, voxel size 1 × 1 × 1 mm3, number of slices 160, sagittal slice orientation, and duration 3 min and 57 s.

4.2.2 Model fitting: non-linear and linear model

Figure 4-1 depicts a typical BOLD response for a representative subject during hypercapnia challenge. On visual inspection, it was observed that the experimental data may not be explained by a linear model or recently suggested sigmoidal model. We hypothesized that the observed BOLD response may be a combination of a linear component and a nonlinear component, where the non-linear component accounts for the observed non-linearity. We used various polynomial functions as a non-linear component in this regression model to fit the data and found that the non-linear component represented by a center shifted cubic function best fit

the data. So the BOLD response to EtCO2 changes is now fitted with new non-linear modeled given by the following equation

$$Y = a + b * X + c * (X - d)^3 \qquad [1]$$

Where a represents initial signal (% BOLD), b represents slope of the linear line (CVR) when non-linearity is accounted for, c is the parameter which represents the non-linearity in BOLD response and d represents the midpoint of non-linear curve. In Equation [1] Y represents the BOLD response and X represents the EtCO2. The parameter c controls the non-linearity of the BOLD response. Figure 4-2 depicts the simulated BOLD response to different c values when all other parameters being same.

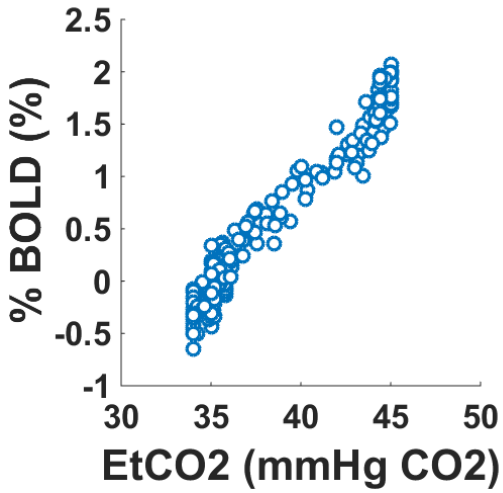

Figure 4-1 BOLD response during hypercapnia stimulus given as a block paradigm for a representative subject. Note that there is a steep rise in BOLD response at the end of the stimulus.

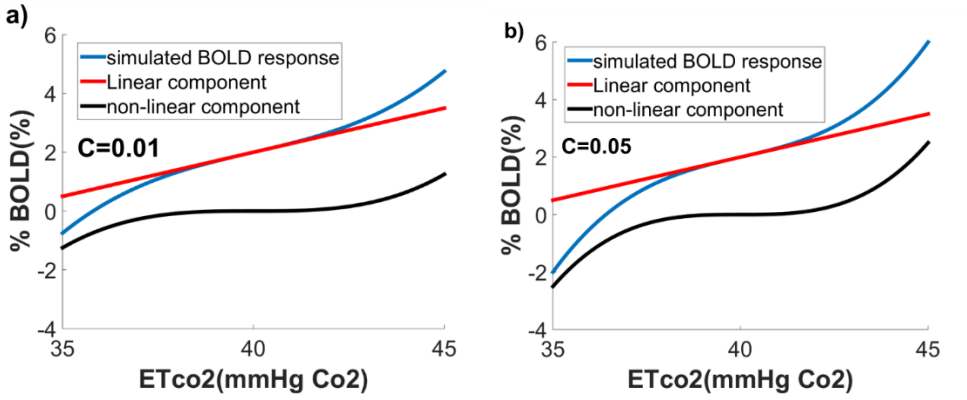

Figure 4-2 Simulated BOLD response using the nonlinear model with different c parameters. a) simulated BOLD response when non-linear parameter C=0.01 and b) simulated BOLD response when non-linear parameter C=0.05. Note that the non-linearity in BOLD response increases with the parameter C.

We additionally fitted the data using a linear model

$$Y = a + b * X \quad [2]$$

Where a represent the y intercept (% BOLD) and b represent slope (% BOLD/mmHg CO_2) i.e. CVR. The BOLD response was fitted using the non-linear and linear model using a least square regression analysis.

4.2.3 Data analysis

The data was processed using in-house MATLAB (Mathworks) scripts. The acquired BOLD images were realigned and smoothed using a Gaussian kernel. Since CSF partial voluming is known to cause additional

nuisance fluctuations in BOLD time series, so a whole brain mask excluding CSF partial voluming was generated. The steps followed for mask generation are as shown in the Figure 4-3. First, the high resolution MPRAGE image was first segmented into gray matter, white and CSF probability maps using statistical parametric mapping (SPM8) software. Then gray and white matter maps were combined together to form gray-white matter mask. In the next step MPRAGE image was coregistered to the BOLD images and resulting transformation matrix was then applied to gray-white matter mask. This would result in gray-white matter mask in subject space. The resulting brain mask used to generate BOLD time course.

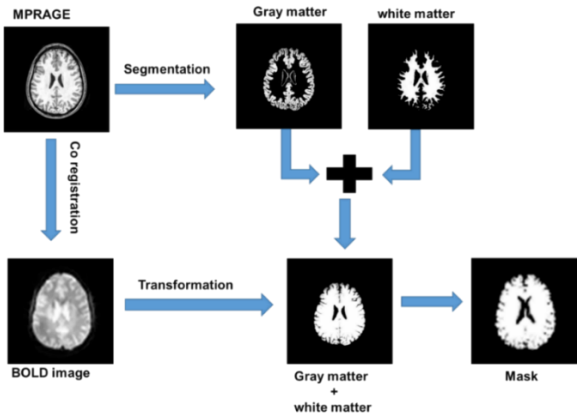

Figure 4-3 Steps involved in generation of white + gray matter mask using MPRAGE image. First MPRAGE image is segmented into white and gray matter image. The MPRAGE image is coregistered with BOLD image in subject space. The resulting transformation matrix from the previous step is applied onto combined gray white matter mask which would final mask in subject space.

EtCO2 time courses were generated that were synchronized with MRI acquisition time (TR). EtCO2 time course represents an input function to the vascular system as the hypercapnia-induced vasodilatation is modulated by the changes in blood CO_2 level. The BOLD time course resulting from the previously described step is the output signal, and it lags behind the input EtCO2 signal, this lag is characteristic of individual physiology. The EtCO2 is shifted to match the BOLD signal. The BOLD time series was first drift corrected. The drift corrected BOLD timeseries data was subtracted with mean baseline (fist 20 points in the time course) BOLD signal and then normalized to the mean intensity of the baseline signal. The resulting BOLD timeseries data were represented in terms of %ΔBOLD from baseline. The baseline EtCO2 was calculated by averaging the first 20 points in the EtCO2 time course.

4.2.4 Statistical analysis

Goodness of fit (r^2) between 2 models used in this study was compared using a student ttest. A p value less than 0.05 was considered significant. Mean ± standard error was also calculated for C and a one sample ttest was performed to check the significance. A correlation analysis was performed to find the age related changes to the fitted parameters and EtCO2. The trend was considered significant only if the p value of these trends was less than 0.05.

4.3 Results

All the subjects who participated in this study successfully completed this study. The average baseline EtCO2 was 39±4 mmHg CO_2 and the mean EtCO2 increase was 9±2 mmHg CO_2. We looked at the age related changes to EtCO2. Figure 4-4 shows the scatter plot between baseline EtCO2 vs age. It can be observed that the baseline EtCO2 decreases with age. The decline rate of EtCO2 is 0.35 mmHg CO_2 per decade and this decline is statistically significant (r^2=0.02, p<0.05).

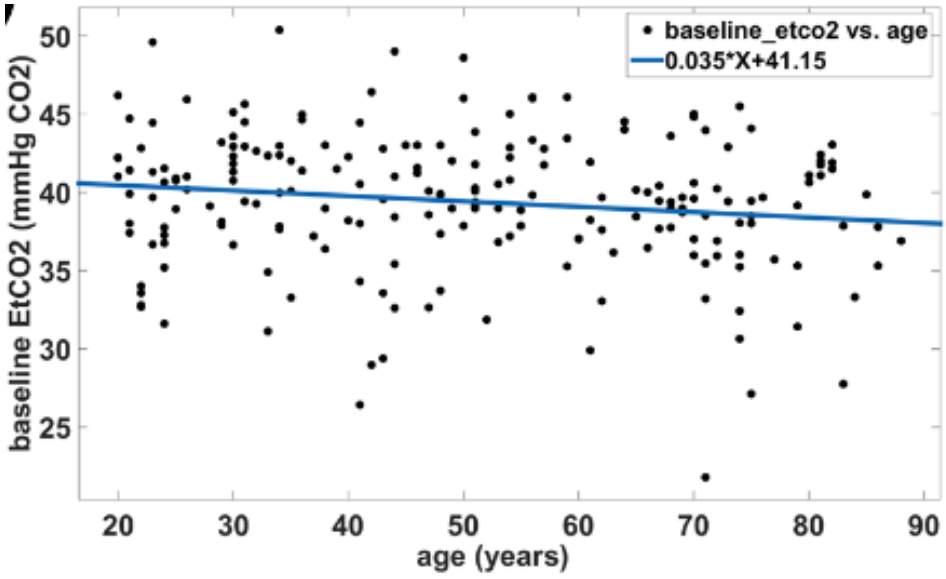

Figure 4-4 Scatter plot of EtCO2 changes with age for baseline EtCO2

We then evaluated gender specific differences to EtCO2 changes with age. Shown in the Figure 4-6 are age related differences between male and female in baseline EtCO2. It can observed from Figure 4-5 the baseline

EtCO2 in male shows significant decrease of 1 mmHg CO_2 per decade (r^2=0.19, p<0.000001) and for females we don't see such age related differences.

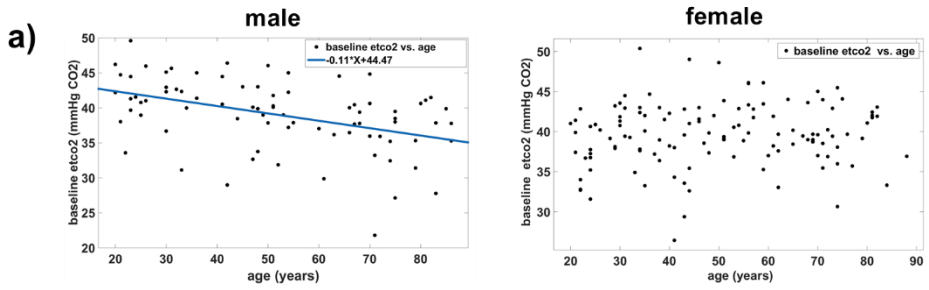

Figure 4-5 Scatter plot baseline EtCO2 with age plotted separately with age.

We then compared the goodness of fit between linear and non-linear model. The age related variation of r^2 is shown in Figure.4-6a) for non-linear model. There was a small decrease in the r^2 with age and this trend was statistically significant (r^2=0.04, p<0.005). Similar trend was observed for r^2 in linear model. Comparing the average r^2 of linear model with nonlinear it was found that nonlinear model (Figure 4-6b)) r^2 was higher than linear model (r^2 (nonlinear) =0.88±0.005, r^2 (linear) =0.87±0.006, p<0.0005).

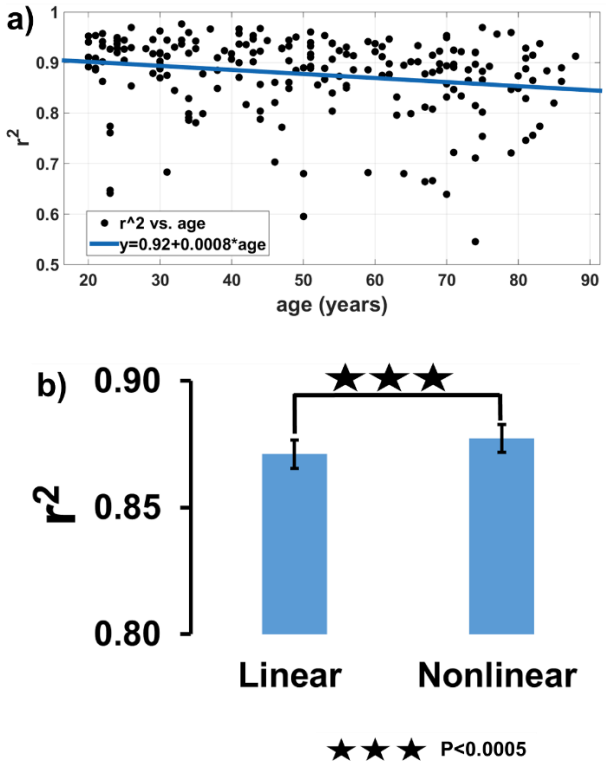

Figure 4-6 Plot illustrates the age related changes of r^2 and comparison of r^2 for both the models. a) Age related changes in r^2, b) comparision of r^2 for both linear and nonlinear model. The error bar represents standard error.

We then investigated the age related changes to fitted parameters. Age related changes for fitted parameters in non-linear model is shown in Figure 4-7. Shown in Figure 4-7a) the age related changes observed for parameter “a” which is a constant. It can be observed that the parameter “a” increases with age at rate of 0.5 % BOLD per decade (r^2=0.16, p<0.000001). The age related variations for parameter b which represents

CVR is shown in Figure 4-7b). The parameter b decreases with age at a rate of 0.001 % BOLD/mmHg CO_2/year (r^2=0.17, p<0.000001). The parameter c which controls the nonlinearity of the BOLD response is depicted in Figure 4-7c). Interestingly, no age related changes were observed in the nonlinearity. The age related changes of parameter d is plotted in Figure 4-7d). The parameter d, which represents midpoint of fitted curve also showed no age related changes.

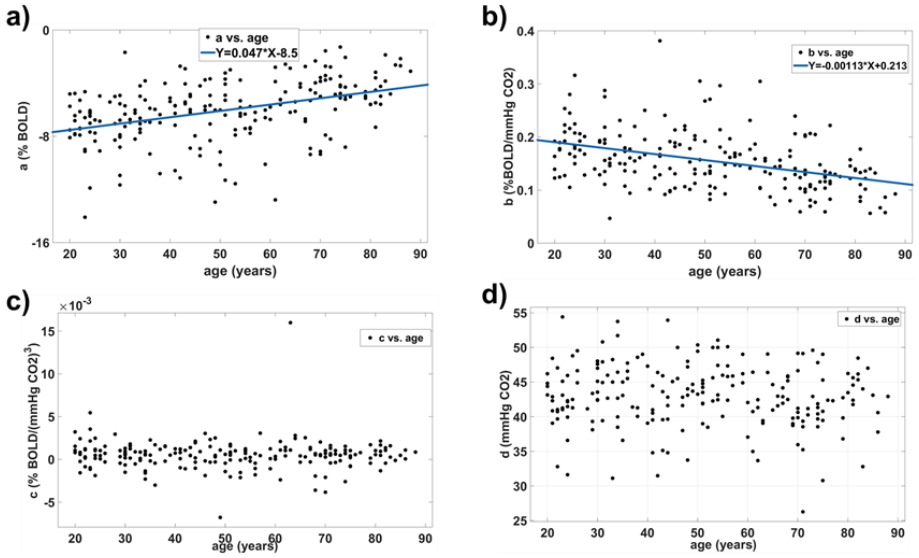

Figure 4-7 Age related variations in fitted parameters for nonlinear model. a) parameter a (constant), b) parameter b (CVR), c) parameter c which represents the nonlinearity in BOLD response and d) parameter d representing the midpoint of the fitted curve.

Even though the parameter c did not show any age related changes, however on average the nonlinearity was significantly (p<0.0005) greater

than zero, c=0.0005±0.0001 (Figure 4-8). When a male participant nonlinearity factor c was compared with female participant, male (0.0008±0.0002) showed a trend of higher c than female (0.0004±0.0001), but this trend was not significant.

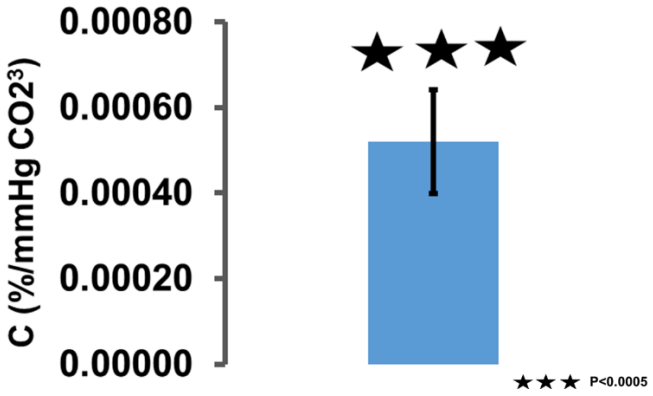

Figure 4-8 Bar plot represents the average c value across all the subjects. The error bar represents standard error. Note that the c was significantly greater than zero.

4.4 Discussion

In this study the nonlinearity of BOLD response to EtCO2 change was investigated for moderate hypercapnia. Contrary to much hypothesized sigmoidal response, we observed opposite pattern i.e. inverse sigmoid pattern in BOLD response. A new biophysical model was proposed to account for this non-linearity. We found that the new proposed non-linear model showed improved r^2, which is an indicator of good ness of fit for a model. This would suggest that the new proposed model better describes

the BOLD response. We found that the non-linearity could be observed in the BOLD response irrespective of age and this non-linearity is significantly greater than zero, suggesting the nonlinearity may be governed by other factors independent of aging. We also found significant age related changes to EtCO2 and these changes were mostly driven by the changes in the male population.

Previous reports on the nonlinearity of the BOLD response using TCD experiments show that BOLD response with progressive ramp stimulus is sigmoidal in nature. In this study we observed that the BOLD response for moderate hypercapnia stimulus mostly follows an inverse sigmoidal shape as shown in Figure 4-1. The exact physiological mechanism of this BOLD response changes is not yet completely understood.

4.4.1 Modeling non-linearity in BOLD response during hypercapnia challenge

During hypercapnia challenge, the quantitative relationship between EtCO2 and BOLD can be modeled by two major steps. One is the effect of EtCO2 changes on CBF (CBF effect). The other is the effect of CBF changes on the BOLD signal (BOLD effect). The non-linearity in the final relationship between BOLD and EtCO2 could be either due to CBF effect or BOLD effect or the combination of both. The first step, i.e. EtCO2 vs.

CBF, has been discussed above. The second step, i.e. the relationship between CBF and BOLD response, is well documented in the literature (Davis et al., 1998; Hoge et al., 1999). We first did a simulation study to investigate the relation between BOLD response and CBF change using the model given by Hoge et al. (Hoge et al., 1999), which is given by the following equation

$$\frac{\Delta S}{S}|_{BOLD} = M\left(1 - \left(\frac{CBF}{CBF_0}\right)^{\alpha-\beta}\right) \quad [3]$$

in which the calibration factor

$$M = TE * A * CBV_0\left[Hct\left(1 - Y_{v,0}\right)\right] \quad [4]$$

Where TE and A are related to imaging parameters and magnetic field strength respectively; CBV_0, CBF_0 and $Y_{v,0}$ represent baseline CBV, CBF and Y_v respectively; Hct represents the hematocrit, i.e., percentage red blood cells in the blood; α represents the grubbs coefficient between CBV and CBF; β represents a coefficient related to vascular geometry. M represents the maximum BOLD signal one can get when all the deoxy hemoglobin molecules are saturated from a voxel (Lu et al., 2008). This equation suggests that we could quantify BOLD response if CBF response is known and vice-versa and the relationship between CBF and BOLD response is non-linear.

Equation [3] suggests that if we know CBF response then we can generate the expected BOLD response. Therefore, to simulate the BOLD response during hypercapnia challenge, we assumed a linear relationship between EtCO2 and CBF, which is given by the following equation

$$CBF = CBF_0 + s * \Delta EtCO_2 * CBF_0 \quad [5]$$

Where CBF_0, s and $\Delta EtCO_2$ represent the baseline CBF, slope (% CBF change with EtCO2 change) and EtCO2 change from baseline. We simulated for the CBF response assuming values of CBF_0 and s found in literature. Figure 4-9a) CBF changes with EtCO2 change. The x-axis represents EtCO2 change from baseline and y axis represents corresponding CBF changes. We then used equation [3] to simulate BOLD response for assumed CBF response in equation [5]. Figure 4-9b) represents the BOLD response for the corresponding CBF changes. It can be observed that the BOLD response starts digressing from linearity with small changes in EtCO2 and it tends to saturate for severe hypercapnia stimulus. The simulated BOLD response shown in Figure 4-2 follows opposite pattern i.e. the BOLD response doesn't saturate, but instead there is an accelerated increase in BOLD response after a certain amount of EtCO2 change. This data suggest that the CBF response required to elicit BOLD response observed in Figure 4-2 could be non-linear.

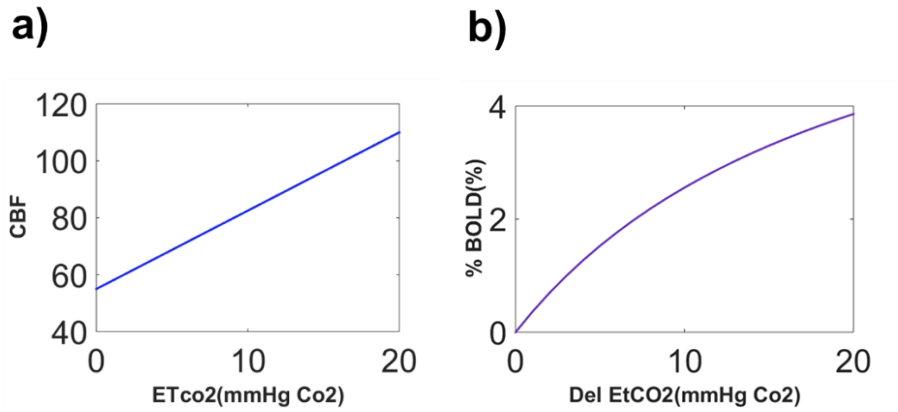

Figure 4-9 CBF and BOLD responses, when linear relationship is assumed between CBF and EtCO2 changes. a) CBF response, b) BOLD response.

Because, we only measured BOLD response in this study, thus, we lack the information pertaining to CBF response. Therefore, we did a simulation to understand the CBF response required to elicit observed BOLD response in Figure 4-1. We simulated for the expected CBF response for this experimental BOLD response by rearranging equation [3].

$$\frac{CBF}{CBF_0} = \left(1 - \frac{\frac{\Delta s}{s}|_{BOLD}}{M}\right)^{\frac{1}{\alpha-\beta}} \quad [6]$$

$$\frac{\Delta s}{s}|_{BOLD} = f(EtCO2) \quad [7]$$

$$\frac{CBF}{CBF_0} = \left(1 - \frac{f(EtCO2)}{M}\right)^{\frac{1}{\alpha-\beta}} \quad [8]$$

Equation [3] could be rewritten as equation [6] and now equation [6] represents CBF as a function of BOLD signal. But we already know that the

BOLD response we observed in Figure 4-1 is a function of EtCO2 (equation [7]) and we hypothesize that the best function to represent the relationship between EtCO2 and BOLD response is given by equation [1]. Substituting equation [7] in [6] the CBF response could be written as a function of EtCO2 (equation [8]). The simulated CBF response using equation [8] is as shown in Figure 4-10 below. The result shown in Figure 4-10, therefore, represent the CBF response required to evoke the experimentally observed BOLD response (Figure 4-1). The simulation result suggests that the CBF response behaves exponentially with changes in EtCO2 contrary to much believed sigmoidal or linear response. In fact various reports using TCD have already shown exponential change to CBF during hypercapnia challenge (Kastrup et al., 1997; Markwalder et al., 1984).

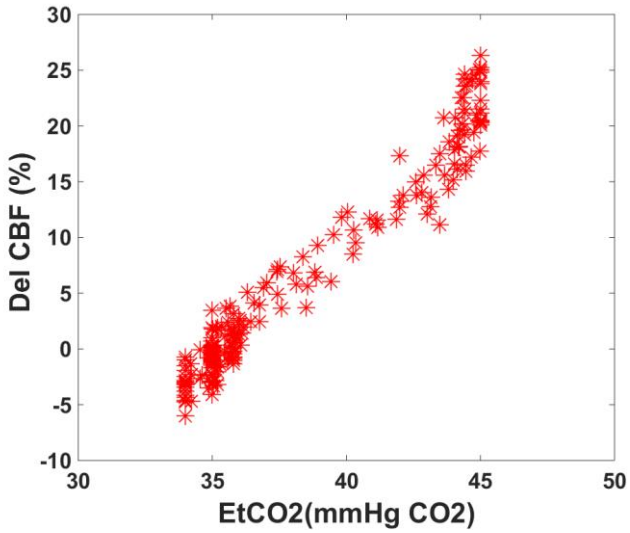

Figure 4-10 Expected CBF response for observed experimental BOLD response (Figure 4-2) for a representative subject.

The BOLD signal changes in response to EtCO2 change observed during hypercapnia challenge is modulated by two mechanisms. First, EtCO2 changes modulates CBF changes (CBF effect), then these CBF changes modulates the BOLD response (BOLD effect). So during hypercapnia challenge, two steps are acting together that could cause a non-linearity in the relationship between BOLD and EtCO2. Interestingly, these two steps have opposite signs in their non-linearity. Thus, the fitted non-linearity parameter indicates whether CBF effect or BOLD effect is dominant. For example, if CBF effect is dominant, this would prevail over the BOLD effect and we will observe an exponential increase in BOLD

response and non-linearity parameter would be positive. When non-linearity parameter c is negative, saturated BOLD response is observed.

We observed that baseline EtCO2 decreases with age and these age related changes are mostly driven by the changes in male population. The reasons for the gender specific differences in the age related changes to EtCO2 is thought to be more physiological in nature than pulmonary function (Anderson et al., 1999). Sex hormones, especially in women have been shown to play important in modulating EtCO2 (Regensteiner et al., 1989). Previous studies have reported that estrogen administration decreases EtCO2 in women (Orr-Walker et al., 1999; Preston et al., 2009), so the decrease in circulating concentrations estrogen post menopause might be counteracting the forces operating to decrease $EtCO_2$ with age. In contrast, administration of testosterone in men has been shown to have no effect on EtCO2 (White et al., 1985), implying EtCO2 in male population are not affected by age related changes in hormones. However, age related decrease in EtCO2 in men was also observed previously (Anderson et al., 1999; Frassetto and Sebastian, 1996). It was suggested respiration adaptation to metabolic acidosis could be the reason for decrease in EtCO2 with age in men (Frassetto and Sebastian, 1996).

The goodness of fit dictates how well a fitted model explains the observed data. It is influenced by the degrees of freedom available during

the regression. So for a linear (two dependent variable) versus a non-linear model (having four dependent variables), it is possible to use an adjusted r^2, which takes into account the number of fit parameters and data-points (DRAPER and Harry, 1998). The high number of acquired data-points (211 time points), used in this study to fit the model reduces the risk of over-fitting our data using a four parameter model, and the differences between fitted and adjusted r^2 values were found to be minimal. Thus, the fitted r^2 for the linear and exponential model was an appropriate measure for comparing the goodness of fit.

The main caveat of this study is its cross-sectional nature, which is known to be susceptible to recruitment bias. In cross-sectional aging studies, we are comparing a typical 20 years old to “super-normal” 80 years old, which may under-estimate the extent of age-changes.

In conclusion, we proposed new biophysical model which could better define BOLD response to hypercapnia stimulus. We showed that this model improves the accuracy compared to linear model used in the literature. Furthermore, we evaluated the age related changes in EtCO2. The availability of such a new model could improve the accuracy BOLD based CVR measurements.

Chapter 5

Conclusion and Outlook

Recently, there is lot of interest in the field for CVR mapping as it reflects the vitality of cerebrovascular function. As such, it has been used as a tool to understand and evaluate many cerebral and cerebrovascular pathologies and also as a prognostic marker for many pathologic condition. Additionally, it has been used as a tool to study the effects of drugs on cerebrovascular and presurgical planning. Recently, there is a new evidence in the literature that the CVR could be used for patient management in ischemic patients. This suggests that the CVR is an important biomarker for cerebrovascular physiology. It can be expected that this technique would be used as an important tool in routine clinical setting. BOLD based CVR measurement most commonly used technique. However, the current method suffers from several limitations related to specificity, sensitivity, and physiological modeling of the measured signal. We sought to improve on these aspects and ultimately provide a clinically-ready CVR imaging procedure that could be immediately translational.

In Aim 1, we developed an optimized BOLD imaging protocol that allowed for the removal of negative signal artifacts in CVR mapping. We showed that, when the signal intensities in CSF and blood compartment are equated, the artifactually negative CVR can be minimized. We have further

showed that sensitvity and reproducibility of the CVR results when using the optimized protocols are comparable to those using the standard protocol. Overall, we recommend the use of a TE of 20-23 ms for BOLD-based CVR mapping, as opposed to the 30-40 ms range commonly used in brain activation fMRI studies. The availability of such a protocol may improve the interpretability of CVR results in clinical settings.

In Aim 2, we took advantage of new multiband (MB) EPI acquisition to improve the sensitivity of BOLD based CVR measurement. We showed that the sensitivity of MB scans was higher compared to conventional EPI scans owing to faster data acquisition rate. We found that sensitivity reduction when moving from a standard resolution scan to high resolution scan was lower in MB scans compared to conventional EPI scan. Furthermore, we found that the sensitivity of multiband scan was similar to conventional EPI scan with double the scan time. The availability of a sensitive technique would further encourage clinicians to adopt the use of CVR for future clinical applications.

In general a linear relationship is assumed between EtCO2 and CBF/BOLD response. However, recent reports using TCD and MRI has shown that CBF/BOLD response show a non-linear behavior with progressive ramp stimulus. The presence non-linearity would comprise the interpretability of CVR results generated using linear model. Moreover, non-

linear characteristic of BOLD response has not yet been investigated for moderate hypercapnia challenge. In Aim3, we investigated the non-linearity in BOLD response during moderate hypercapnia challenge. We proposed a new biophysical model that incorporates possible nonlinearity while preserving the linear effect. Furthermore, we evaluated the age related changes in EtCO2. The availability of such a new model could improve the accuracy BOLD based CVR measurements.

There are still few challenges that have to be overcome before this powerful tool can be used for routine clinical applications. Hypercapnia gas is known to cause neuronal suppression and these potential effects on neurometabolism could complicate the findings of CVR measurements. However, recently a new iso-metabolic gas mixture was proposed which could counter act this suppression effect. In future, the new iso-metabolic gas mixture could be used for CVR experiments. Furthermore, the multiband acquisition has been shown to have signal leakage between simultaneously excited slices and this leakage has been shown to increase with higher acceleration factor. Signal leakage could be a confounding factor for sensitivity improvement at higher acceleration factor. However, recently it has been shown that use of Split Slice-GRAPPA reconstruction could significantly reduce this signal leakage.

References

Alexander, S.C., Wollman, H., Cohen, P.J., Chase, P.E., Behar, M., 1964. Cerebrovascular Response to Paco2 during Halothane Anesthesia in Man. J Appl Physiol 19, 561-565.

Anderson, D.E., Parsons, D.J., Scuteri, A., 1999. End tidal CO2 is an independent determinant of systolic blood pressure in women. Journal of hypertension 17, 1073-1080.

Battisti-Charbonney, A., Fisher, J., Duffin, J., 2011. The cerebrovascular response to carbon dioxide in humans. J Physiol 589, 3039-3048.

Bayliss, W.M., 1902. On the local reactions of the arterial wall to changes of internal pressure. The Journal of physiology 28, 220-231.

Bhogal, A.A., Siero, J.C., Fisher, J.A., Froeling, M., Luijten, P., Philippens, M., Hoogduin, H., 2014. Investigating the non-linearity of the BOLD cerebrovascular reactivity response to targeted hypo/hypercapnia at 7T. Neuroimage 98, 296-305.

Blockley, N.P., Driver, I.D., Francis, S.T., Fisher, J.A., Gowland, P.A., 2011. An improved method for acquiring cerebrovascular reactivity maps. Magn. Reson. Med. 65, 1278-1286.

Bulte, D.P., Drescher, K., Jezzard, P., 2009. Comparison of hypercapnia-based calibration techniques for measurement of cerebral oxygen metabolism with MRI. Magn Reson Med 61, 391-398.

Caceres, A., Hall, D.L., Zelaya, F.O., Williams, S.C., Mehta, M.A., 2009. Measuring fMRI reliability with the intra-class correlation coefficient. Neuroimage 45, 758-768.

Chen, L., Bernstein, M., Huston, J., Fain, S., 2001. Measurements of T1 relaxation times at 3.0 T: implications for clinical MRA. Proceedings of the 9th Annual Meeting of ISMRM, Glasgow, Scotland.

Claassen, J.A., Zhang, R., Fu, Q., Witkowski, S., Levine, B.D., 2007. Transcranial Doppler estimation of cerebral blood flow and cerebrovascular conductance during modified rebreathing. J Appl Physiol (1985) 102, 870-877.

Clare, S., Jezzard, P., 2001. Rapid T(1) mapping using multislice echo planar imaging. Magn Reson Med 45, 630-634.

Davis, T.L., Kwong, K.K., Weisskoff, R.M., Rosen, B.R., 1998. Calibrated functional MRI: mapping the dynamics of oxidative metabolism. Proc Natl Acad Sci U S A 95, 1834-1839.

de Zwart, J.A., Gelderen, P., Fukunaga, M., Duyn, J.H., 2008. Reducing correlated noise in fMRI data. Magn Reson Med 59, 939-945.

Donald, M., Paterson, B., 2006. End tidal carbon dioxide monitoring in prehospital and retrieval medicine: a review. Emergency medicine journal 23, 728-730.

DRAPER, N.R., Harry, S., 1998. Applied regression analysis.

Feinberg, D.A., Moeller, S., Smith, S.M., Auerbach, E., Ramanna, S., Glasser, M.F., Miller, K.L., Ugurbil, K., Yacoub, E., 2010. Multiplexed Echo Planar Imaging for Sub-Second Whole Brain FMRI and Fast Diffusion Imaging. PLoS ONE 5, e15710.

Fierstra, J., Spieth, S., Tran, L., Conklin, J., Tymianski, M., ter Brugge, K.G., Fisher, J.A., Mikulis, D.J., Krings, T., 2011. Severely impaired cerebrovascular reserve in patients with cerebral proliferative angiopathy. J Neurosurg Pediatr. 8, 310-315.

Frassetto, L., Sebastian, A., 1996. Age and systemic acid-base equilibrium: analysis of published data. J Gerontol A Biol Sci Med Sci 51, B91-99.

Gauthier, C.J., Desjardins-Crepeau, L., Madjar, C., Bherer, L., Hoge, R.D., 2012. Absolute quantification of resting oxygen metabolism and metabolic reactivity during functional activation using QUO2 MRI. Neuroimage 63, 1353-1363.

Gauthier, C.J., Hoge, R.D., 2013. A generalized procedure for calibrated MRI incorporating hyperoxia and hypercapnia. Hum Brain Mapp 34, 1053-1069.

Glodzik, L., Randall, C., Rusinek, H., de Leon, M.J., 2013. Cerebrovascular reactivity to carbon dioxide in Alzheimer's disease. J Alzheimers Dis 35, 427-440.

Greenberg, S.M., 2006a. Small vessels, big problems. N Engl J Med 354, 1451-1453.

Greenberg, S.M., 2006b. Small vessels, big problems. N Engl J Med. 354, 1451-1453.

Grubb, R.L., Jr., Raichle, M.E., Eichling, J.O., Ter-Pogossian, M.M., 1974. The effects of changes in PaCO2 on cerebral blood volume, blood flow, and vascular mean transit time. Stroke 5, 630-639.

Gupta, A., Chazen, J.L., Hartman, M., Delgado, D., Anumula, N., Shao, H., Mazumdar, M., Segal, A.Z., Kamel, H., Leifer, D., Sanelli, P.C., 2012. Cerebrovascular reserve and stroke risk in patients with carotid stenosis or occlusion: a systematic review and meta-analysis. Stroke 43, 2884-2891.

Han, J.S., Abou-Hamden, A., Mandell, D.M., Poublanc, J., Crawley, A.P., Fisher, J.A., Mikulis, D.J., Tymianski, M., 2011. Impact of extracranial-intracranial bypass on cerebrovascular reactivity and clinical outcome in patients with symptomatic moyamoya vasculopathy. Stroke 42, 3047-3054.

Han, J.S., Mandell, D.M., Poublanc, J., Mardimae, A., Slessarev, M., Jaigobin, C., Fisher, J.A., Mikulis, D.J., 2008. BOLD-MRI cerebrovascular reactivity findings in cocaine-induced cerebral vasculitis. Nat Clin Pract Neurol 4, 628-632.

Harrison, R.V., Harel, N., Panesar, J., Mount, R.J., 2002. Blood capillary distribution correlates with hemodynamic-based functional imaging in cerebral cortex. Cerebral Cortex 12, 225-233.

Henson, R., 2005. Efficient Experimental Design for fMRI. Statistical Parametric Mapping: The Analysis of Functional Brain Images. Elsevier/Academic Press.

Hoge, R.D., Atkinson, J., Gill, B., Crelier, G.R., Marrett, S., Pike, G.B., 1999. Investigation of BOLD signal dependence on cerebral blood flow and oxygen consumption: the deoxyhemoglobin dilution model. Magn Reson Med 42, 849-863.

Johnston, A.J., Steiner, L.A., Gupta, A.K., Menon, D.K., 2003. Cerebral oxygen vasoreactivity and cerebral tissue oxygen reactivity. Br J Anaesth 90, 774-786.

Karapanayiotides, T., Piechowski-Jozwiak, B., Van Melle, G., Bogousslavsky, J., Devuyst, G., 2004. Stroke patterns, etiology, and prognosis in patients with diabetes mellitus. Neurology 62, 1558-1562.

Kassner, A., Winter, J.D., Poublanc, J., Mikulis, D.J., Crawley, A.P., 2010. Blood-oxygen level dependent MRI measures of cerebrovascular reactivity using a controlled respiratory challenge: reproducibility and gender differences. J Magn Reson Imaging 31, 298-304.

Kastrup, A., Kruger, G., Neumann-Haefelin, T., Moseley, M.E., 2001. Assessment of cerebrovascular reactivity with functional magnetic resonance imaging: comparison of CO(2) and breath holding. Magn Reson Imaging. 19, 13-20.

Kastrup, A., Thomas, C., Hartmann, C., Schabet, M., 1997. Sex dependency of cerebrovascular CO2 reactivity in normal subjects. Stroke 28, 2353-2356.

Kety, S.S., Schmidt, C.F., 1948. The Effects of Altered Arterial Tensions of Carbon Dioxide and Oxygen on Cerebral Blood Flow and Cerebral Oxygen Consumption of Normal Young Men. J Clin Invest 27, 484-492.

Kuroda, S., Houkin, K., Kamiyama, H., Mitsumori, K., Iwasaki, Y., Abe, H., 2001. Long-term prognosis of medically treated patients with internal carotid or middle cerebral artery occlusion: can acetazolamide test predict it? Stroke 32, 2110-2116.

Lassen, N.A., 1959. Cerebral blood flow and oxygen consumption in man. Physiol Rev 39, 183-238.

Leoni, R.F., Mazzetto-Betti, K.C., Silva, A.C., dos Santos, A.C., de Araujo, D.B., Leite, J.P., Pontes-Neto, O.M., 2012. Assessing cerebrovascular reactivity in carotid steno-occlusive disease using MRI BOLD and ASL techniques. Radiology research and practice 2012.

Li, L., Zeng, L., Lin, Z.-J., Cazzell, M., Liu, H., 2015. Tutorial on use of intraclass correlation coefficients for assessing intertest reliability and its application in functional near-infrared spectroscopy–based brain imaging. Journal of biomedical optics 20, 050801-050801.

Liu, P., , Y.L., , H.L., 2014. Normalizing cerebrovascular reactivity map via concomitant CO2 and O2 challenge. Proceedings of the 9th Annual Meeting of ISMRM, Milan,Italy,.

Lu, H., Clingman, C., Golay, X., van Zijl, P.C., 2004a. Determining the longitudinal relaxation time (T1) of blood at 3.0 Tesla. Magn Reson Med 52, 679-682.

Lu, H., Golay, X., Pekar, J.J., Van Zijl, P.C., 2004b. Sustained poststimulus elevation in cerebral oxygen utilization after vascular recovery. J Cereb Blood Flow Metab 24, 764-770.

Lu, H., Golay, X., van Zijl, P.C., 2002. Intervoxel heterogeneity of event-related functional magnetic resonance imaging responses as a function of T(1) weighting. Neuroimage 17, 943-955.

Lu, H., van Zijl, P.C., 2005. Experimental measurement of extravascular parenchymal BOLD effects and tissue oxygen extraction fractions using multi-echo VASO fMRI at 1.5 and 3.0 T. Magn Reson Med 53, 808-816.

Lu, H., Zhao, C., Ge, Y., Lewis-Amezcua, K., 2008. Baseline blood oxygenation modulates response amplitude: Physiologic basis for

intersubject variations in functional MRI signals. Magn Reson Med 60, 364-372.

Mandell, D.M., Han, J.S., Poublanc, J., Crawley, A.P., Kassner, A., Fisher, J.A., Mikulis, D.J., 2008a. Selective reduction of blood flow to white matter during hypercapnia corresponds with leukoaraiosis. Stroke 39, 1993-1998.

Mandell, D.M., Han, J.S., Poublanc, J., Crawley, A.P., Stainsby, J.A., Fisher, J.A., Mikulis, D.J., 2008b. Mapping cerebrovascular reactivity using blood oxygen level-dependent MRI in Patients with arterial steno-occlusive disease: comparison with arterial spin labeling MRI. Stroke 39, 2021-2028.

Markwalder, T.M., Grolimund, P., Seiler, R.W., Roth, F., Aaslid, R., 1984. Dependency of blood flow velocity in the middle cerebral artery on end-tidal carbon dioxide partial pressure--a transcranial ultrasound Doppler study. J Cereb Blood Flow Metab 4, 368-372.

Meng, L., Gelb, A.W., 2015. Regulation of cerebral autoregulation by carbon dioxide. Anesthesiology 122, 196-205.

Mikulis, D.J., Krolczyk, G., Desal, H., Logan, W., deVeber, G., Dirks, P., Tymianski, M., Crawley, A., Vesely, A., Kassner, A., 2005. Preoperative and postoperative mapping of cerebrovascular reactivity in moyamoya disease by using blood oxygen level-dependent magnetic resonance imaging. Journal of neurosurgery 103, 347-355.

Murphy, K., Bodurka, J., Bandettini, P.A., 2007. How long to scan? The relationship between fMRI temporal signal to noise ratio and necessary scan duration. Neuroimage 34, 565-574.

Ogasawara, K., Ito, H., Sasoh, M., Okuguchi, T., Kobayashi, M., Yukawa, H., Terasaki, K., Ogawa, A., 2003. Quantitative measurement of regional cerebrovascular reactivity to acetazolamide using 123I-N-isopropyl-p-iodoamphetamine autoradiography with SPECT: validation study using H2 15O with PET. J Nucl Med 44, 520-525.

Ogawa, S., Lee, T.M., Kay, A.R., Tank, D.W., 1990. Brain magnetic resonance imaging with contrast dependent on blood oxygenation. Proc Natl Acad Sci U S A 87, 9868-9872.

Oremus, M., Oremus, C., Hall, G.B., McKinnon, M.C., Ect, Cognition Systematic Review, T., 2012. Inter-rater and test-retest reliability of quality assessments by novice student raters using the Jadad and Newcastle-Ottawa Scales. BMJ Open 2.

Orr-Walker, B.J., Horne, A.M., Evans, M.C., Grey, A.B., Murray, M.A., McNeil, A.R., Reid, I.R., 1999. Hormone replacement therapy causes a respiratory alkalosis in normal postmenopausal women. J Clin Endocrinol Metab 84, 1997-2001.

Osol, G., Brekke, J.F., McElroy-Yaggy, K., Gokina, N.I., 2002. Myogenic tone, reactivity, and forced dilatation: a three-phase model of in vitro

arterial myogenic behavior. Am J Physiol Heart Circ Physiol 283, H2260-2267.

Pattinson, K.T., Rogers, R., Mayhew, S.D., Tracey, I., Wise, R.G., 2007. Pharmacological FMRI: measuring opioid effects on the BOLD response to hypercapnia. J Cereb Blood Flow Metab 27, 414-423.

Paulson, O.B., Strandgaard, S., Edvinsson, L., 1990. Cerebral autoregulation. Cerebrovasc Brain Metab Rev 2, 161-192.

Peterson, E.C., Wang, Z., Britz, G., 2011. Regulation of cerebral blood flow. Int J Vasc Med 2011, 823525.

Posse, S., Ackley, E., Mutihac, R., Rick, J., Shane, M., Murray-Krezan, C., Zaitsev, M., Speck, O., 2012. Enhancement of temporal resolution and BOLD sensitivity in real-time fMRI using multi-slab echo-volumar imaging. Neuroimage 61, 115-130.

Preibisch, C., Castrillon, G.J., Buhrer, M., Riedl, V., 2015. Evaluation of Multiband EPI Acquisitions for Resting State fMRI. PLoS ONE 10, e0136961.

Preston, M.E., Jensen, D., Janssen, I., Fisher, J.T., 2009. Effect of menopause on the chemical control of breathing and its relationship with acid-base status. Am J Physiol Regul Integr Comp Physiol 296, R722-727.

Ramsey, N.F., Kirkby, B.S., Van Gelderen, P., Berman, K.F., Duyn, J.H., Frank, J.A., Mattay, V.S., Van Horn, J.D., Esposito, G., Moonen, C.T.,

Weinberger, D.R., 1996. Functional mapping of human sensorimotor cortex with 3D BOLD fMRI correlates highly with H2(15)O PET rCBF. J Cereb Blood Flow Metab 16, 755-764.

Ravi, H., Thomas, B.P., Peng, S.L., Liu, H., Lu, H., 2015. On the optimization of imaging protocol for the mapping of cerebrovascular reactivity. J Magn Reson Imaging.

Regensteiner, J.G., Woodard, W.D., Hagerman, D.D., Weil, J.V., Pickett, C.K., Bender, P.R., Moore, L.G., 1989. Combined effects of female hormones and metabolic rate on ventilatory drives in women. J Appl Physiol (1985) 66, 808-813.

Rostrup, E., Law, I., Blinkenberg, M., Larsson, H., Born, A.P., Holm, S., Paulson, O., 2000. Regional differences in the CBF and BOLD responses to hypercapnia: a combined PET and fMRI study. Neuroimage 11, 87-97.

Saad, Z.S., Ropella, K.M., DeYoe, E.A., Bandettini, P.A., 2003. The spatial extent of the BOLD response. Neuroimage 19, 132-144.

Setsompop, K., Gagoski, B.A., Polimeni, J.R., Witzel, T., Wedeen, V.J., Wald, L.L., 2012. Blipped-controlled aliasing in parallel imaging for simultaneous multislice echo planar imaging with reduced g-factor penalty. Magn Reson Med 67, 1210-1224.

Silvestrini, M., Vernieri, F., Pasqualetti, P., Matteis, M., Passarelli, F., Troisi, E., Caltagirone, C., 2000. Impaired cerebral vasoreactivity and risk

of stroke in patients with asymptomatic carotid artery stenosis. JAMA 283, 2122-2127.

Silvestrini, M., Viticchi, G., Altamura, C., Luzzi, S., Balucani, C., Vernieri, F., 2012. Cerebrovascular assessment for the risk prediction of Alzheimer's disease. J Alzheimers Dis 32, 689-698.

Smielewski, P., Kirkpatrick, P., Minhas, P., Pickard, J.D., Czosnyka, M., 1995. Can cerebrovascular reactivity be measured with near-infrared spectroscopy? Stroke 26, 2285-2292.

St Lawrence, K.S., Ye, F.Q., Lewis, B.K., Weinberger, D.R., Frank, J.A., McLaughlin, A.C., 2002. Effects of indomethacin on cerebral blood flow at rest and during hypercapnia: an arterial spin tagging study in humans. Journal of Magnetic Resonance Imaging 15, 628-635.

Tameem, A., Krovvidi, H., 2013. Cerebral physiology. Continuing Education in Anaesthesia, Critical Care & Pain 13, 113-118.

Thomas, B.P., Liu, P., Aslan, S., King, K.S., van Osch, M.J., Lu, H., 2013. Physiologic underpinnings of negative BOLD cerebrovascular reactivity in brain ventricles. Neuroimage 83, 505-512.

Todd, N., Moeller, S., Auerbach, E.J., Yacoub, E., Flandin, G., Weiskopf, N., 2016. Evaluation of 2D multiband EPI imaging for high-resolution, whole-brain, task-based fMRI studies at 3T: Sensitivity and slice leakage artifacts. Neuroimage 124, 32-42.

Vernieri, F., Pasqualetti, P., Matteis, M., Passarelli, F., Troisi, E., Rossini, P.M., Caltagirone, C., Silvestrini, M., 2001. Effect of collateral blood flow and cerebral vasomotor reactivity on the outcome of carotid artery occlusion. Stroke 32, 1552-1558.

White, D.P., Schneider, B.K., Santen, R.J., McDermott, M., Pickett, C.K., Zwillich, C.W., Weil, J.V., 1985. Influence of testosterone on ventilation and chemosensitivity in male subjects. J Appl Physiol (1985) 59, 1452-1457.

Whittall, K.P., MacKay, A.L., Graeb, D.A., Nugent, R.A., Li, D.K., Paty, D.W., 1997. In vivo measurement of T2 distributions and water contents in normal human brain. Magn Reson Med 37, 34-43.

Xu, J., Moeller, S., Auerbach, E.J., Strupp, J., Smith, S.M., Feinberg, D.A., Yacoub, E., Uğurbil, K., 2013. Evaluation of slice accelerations using multiband echo planar imaging at 3T. Neuroimage 83, 991-1001.

Yezhuvath, U.S., Lewis-Amezcua, K., Varghese, R., Xiao, G., Lu, H., 2009a. On the assessment of cerebrovascular reactivity using hypercapnia BOLD MRI. NMR Biomed 22, 779-786.

Yezhuvath, U.S., Lewis-Amezcua, K., Varghese, R., Xiao, G., Lu, H., 2009b. On the assessment of cerebrovascular reactivity using hypercapnia BOLD MRI. NMR Biomed. 22, 779-786.

Yezhuvath, U.S., Uh, J., Cheng, Y., Martin-Cook, K., Weiner, M., Diaz-Arrastia, R., van Osch, M., Lu, H., 2012. Forebrain-dominant deficit in cerebrovascular reactivity in Alzheimer's disease. Neurobiol Aging 33, 75-82.

Zaca, D., Hua, J., Pillai, J.J., 2011a. Cerebrovascular reactivity mapping for brain tumor presurgical planning. World J Clin Oncol 2, 289-298.

Zaca, D., Hua, J., Pillai, J.J., 2011b. Cerebrovascular reactivity mapping for brain tumor presurgical planning. World J Clin Oncol. 2, 289-298.

Zhao, J.M., Clingman, C.S., Narvainen, M.J., Kauppinen, R.A., van Zijl, P.C., 2007. Oxygenation and hematocrit dependence of transverse relaxation rates of blood at 3T. Magn Reson Med 58, 592-597.

Ziyeh, S., Rick, J., Reinhard, M., Hetzel, A., Mader, I., Speck, O., 2005. Blood oxygen level-dependent MRI of cerebral CO2 reactivity in severe carotid stenosis and occlusion. Stroke 36, 751-756.

Biographical Information

Harshan Ravi, born and brought up in Hyderabad, received his bachelor's degree from Jawahar Lal Nehru Technological University, Hyderabad in Biomedical engineering, in June 2008. After completing his Bachelor's degree he pursued higher education abroad to gain more knowledge in the field. He joined Masters at University of Texas at Arlington, in August 2008, where he joined Dr. Khosrow Behbehani's lab as a graduate research assistant. Here he worked on developing a support vector machine classifier to detect sleep apnea from cardiac events. In September 2011 he was awarded Master's degree. After completing his Masters he joined Dr. Hanzhnag Lu's lab which specialize in developing MRI techniques to understand brain physiology. Here he worked on improving BOLD MRI based technique used for Cerbrovascular reactivity measurements. He was awarded the PhD degree in December 2015. His thesis was titled "MRI of cerebrovascular reactivity using gas inhalation challenges". He plans to pursue a postdoctoral/clinical research scientist position in future.